iScience

CellPress
OPEN ACCESS

Article

Ferroelectric hydrogels from amino acids and oleic acid

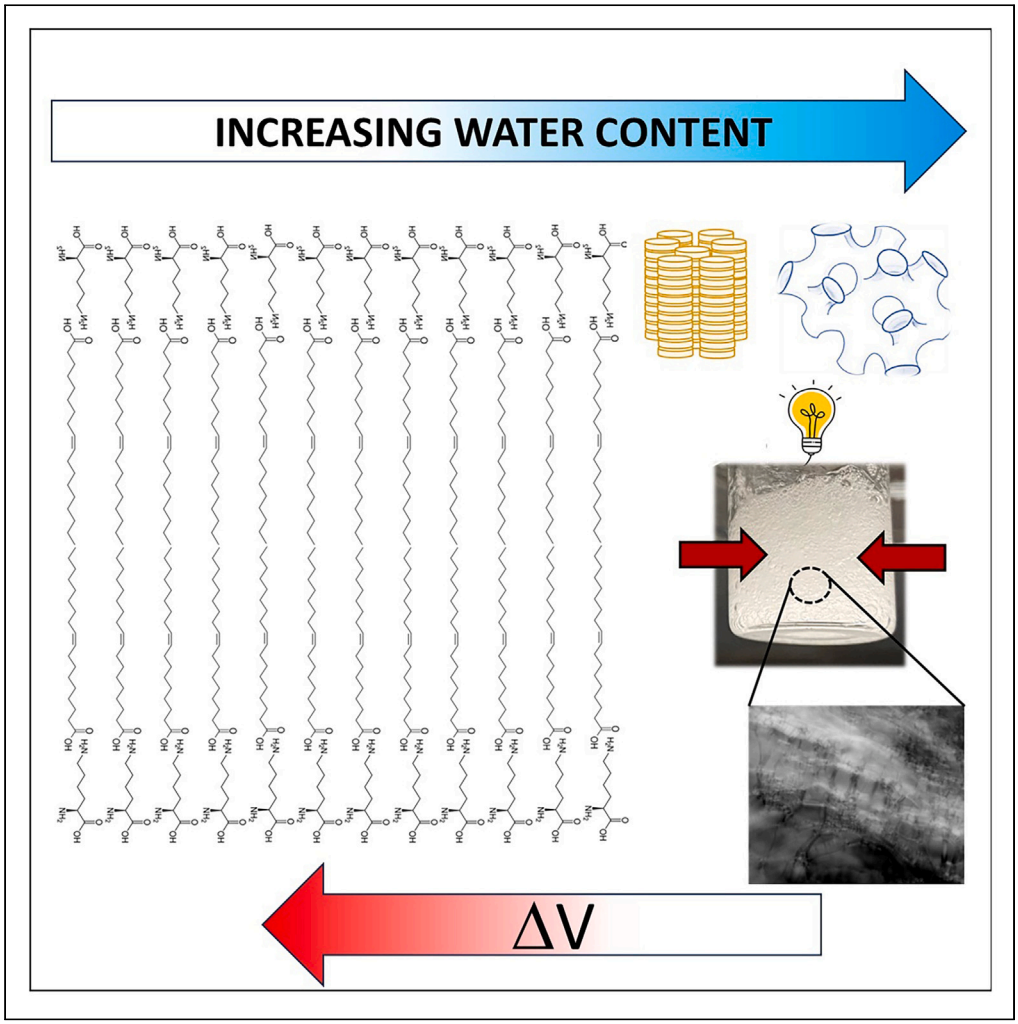

Erica Pensini, Peter Meszaros, Nour Kashlan, ..., Saeed Mirzaee Ghazani, Joshua van der Zalm, Aicheng Chen

epensini@uoguelph.ca

Highlights

Lysine and oleic acid mixtures with 74–85 wt % water are piezoelectric gels

Gels are liquid crystals, with a structure depending on the water content

The structure is lamellar without water and a bi-continuous sponge with 89 wt % water

Electric fields induce crystalline phase transitions from sponge to lamellar

Pensini et al., iScience 27, 110601
September 20, 2024
https://doi.org/10.1016/j.isci.2024.110601

iScience

CellPress
OPEN ACCESS

Article

Ferroelectric hydrogels from amino acids and oleic acid

Erica Pensini,[1,2,6,*] Peter Meszaros,[1] Nour Kashlan,[1] Alejandro G. Marangoni,[2,3] Thamara Laredo,[4] Stefano Gregori,[1] Saeed Mirzaee Ghazani,[3] Joshua van der Zalm,[5] and Aicheng Chen[5]

SUMMARY

Ferroelectric bio-based materials with a high water content (≈90 wt %) were not previously developed. Here, we develop hydrogels containing ≈90 wt % water, amino acids (lysine and arginine) and oleic acid. The NH and CH groups of lysine hydrogen bond water, as shown by attenuated total reflectance-Fourier transform infrared spectroscopy, yielding electrically conductive solutions. Lysine also interacts with oleic acid, yielding hard materials with a lamellar crystal structure, as revealed by synchrotron small angle X-ray scattering. Polarized light microscopy and shear rheology show that aqueous mixtures of amino acids and oleic acid are birefringent gels. These gels have a columnar, hexagonal crystal structure with 54–85 wt % water, and a bi-continuous sponge crystal structure with 89 wt % water. They are piezoelectric, as demonstrated by cyclic voltammetry. Thus, they deform and undergo crystalline phase transitions when exposed to electric fields. The piezoelectric materials developed can find use in medical applications and clean energy harvesting.

INTRODUCTION

Piezoelectric materials are materials able to generate an electrical charge in response to a mechanical stress or deformation (direct piezoelectric effect).[1] They also deform when subjected to an electric field (inverse piezoelectric effect). The piezoelectric effect was first described in 1707 by Johann Georg Schmidt in the book Curiöse Speculationes bey Schalflosen Nächten (Curious Speculations During Sleepless Nights),[2] relevant passages of which have been translated to English.[3]

Piezoelectric materials are harnessed for diverse applications including (but not limited to) pressure sensors, actuators for precise positioning, wireless sensing, clean energy harvesting (achieved by converting mechanical vibrations into electrical energy), self-powered electronic devices and ultrasonic transducers for medical imaging.[1,4–15] In medical applications, they are also used to produce patches that promote healing,[1] for cartilage remodeling,[16] or for wearable devices.[17] Finally, ferroelectric materials have been harnessed to produce catalysts able to enhance the remediation of organic pollutants.[18]

A common characteristic of piezoelectric materials is the lack of symmetry in their crystal structure. This observation was reported in 1880 by Jacques and Pierre Curie, who discovered that a compression of asymmetric inorganic crystals along their hemihedral axes produces electric polarization.[19] Examples of such crystals are quartz and tourmaline (a crystalline silicate gemstone with a range of appealing colors, composed of boron and either aluminum, iron, magnesium, sodium, lithium, or potassium), as well as Rochelle salt.[20,21] The Curie brothers also observed that the effect of compressing and expanding asymmetric crystals along their hemihedral axes is similar to that of cooling and heating them (pyroelectricity).[19] Indeed, cooling and heating also deform materials. Extensive experimentation on the pyroelectric behavior of the piezoelectric material tourmaline was conducted in 1859 by Gaugain.[22] The common nature of the pyroelectric and piezoelectric effects was clearly laid out by W.C. Röntgen in 1883.[23]

In addition to inorganic materials, organic materials can be both electrically conductive and piezoelectric. The piezoelectric properties of biological molecules have attracted interest in recent times, for the development of bioelectronic devices.[24] For example, peptide-small molecule conjugates have been used to produce self-assembled organic conductors.[24] In particular, amino acids have been used with conjugated molecules, to produce self-assembled electronically delocalized nanostructures.[24] The dielectric properties of proteins and amino acids in both their solid state and in water have been discussed in an informative series of manuscripts published in the Transactions of the Faraday Society (e.g., studies by Bayley[25] and Gent[26]). In their native environment, proteins conduct mainly through electron transfer, although they also allow short-range electron transport upon integration into solid-state junctions.[24] While proteins conduct electricity in

[1]School of Engineering, University of Guelph, 50 Stone Road East, Guelph, ON N1G 2W1, Canada
[2]Biophysics Interdepartmental Group (BIG), University of Guelph, 50 Stone Road East, Guelph, ON N1G 2W1, Canada
[3]Food Science Department, University of Guelph, 50 Stone Road East, Guelph, ON N1G 2W1, Canada
[4]Chemistry Department, Lakehead University, 500 University Avenue, Orillia, ON L3V 0B9, Canada
[5]Chemistry Department, University of Guelph, 50 Stone Road East, Guelph, ON N1G 2W1, Canada
[6]Lead contact
*Correspondence: epensini@uoguelph.ca
https://doi.org/10.1016/j.isci.2024.110601

both their wet and dry states, the electrical conductivity of proteins markedly increases in the presence of water.[27] Similarly, water layers adsorbed on the surface of peptides promote proton conduction and carboxylic acid side chains act as proton-donors, thereby playing an important role for conductivity.[24] Importantly, many biological materials are highly ordered and have low symmetry, rendering them piezoelectric.[28] For instance, different proteins are piezoelectric, such as collagen in the human body.[29] Bone is composed of collagen and hydroxyapatite ceramics.[29] Mechanical stress on the bone produces electrical signals, which support bone growth, healing, and remodeling. Mechanical stress acting on bones generates an electric potential, which attracts osteogenic cells because of the formation of electric dipoles.[29] Similarly, cartilage, ligament, tendon, skin, and hair are composed of collagen or keratin, both of which are piezoelectric proteins.[29]

This manuscript focuses on amino acids, which are the building blocks of proteins. There are 20 amino acids in total. They are organic compounds containing a carboxyl (-COOH) group, an amine (NH_2) group, hydrogen, and a side functional group which varies for each individual amino acid. Amino acids can form 3D crystal structures. The structures formed dictate if they are piezoelectric. For example, L-enantiomers of amino acids crystallize in either monoclinic or orthorhombic forms, and are piezoelectric.[28] L-tryptophan is an exception, because it is triclinic (P1 symmetry) and it is not piezoelectric.[28] In 1970, Vasilescu et al. had already listed the piezoelectric properties and the crystal structure of different amino acids.[30] The authors reported that L-lysine hydrochloride is piezoelectric.[30] Our manuscript focuses on materials produced with L-lysine. The simplest amino acid is glycine. A recent study published in 2023 used glycine to produce piezoelectric films.[31] While solvent cast films are brittle and have poor piezoelectric properties, the authors produced flexible piezoelectric nanofibers of glycine crystals embedded inside polycaprolactone.[31] In this study, the authors proposed that the piezoelectric properties of the films are due to the stretching and alignment of the nanofibers during the fabrication process. A previous study also analyzed the piezoelectric properties of γ glycine.[32] The authors ascribed the high piezoelectric coefficients of γ glycine to the efficient packing of glycine molecules along specific crystallographic planes and directions.[32] Other authors developed piezoelectric materials using alanine and polyvinyl acetate.[33]

While bio-based materials were described before, previous studies did not develop piezoelectric hydrogels with amino acids and fatty acids, such as those presented in our study. Our hydrogels contain high proportions of water and are completely benign. Therefore, they are suitable for diverse applications, ranging from clean energy production to medical applications, to enhance healing of damaged tissues. Here, we describe such materials, exploring the molecular interactions occurring between their components, their structure both in the absence and in the presence of applied electric fields, as well as their piezoelectric properties.

RESULTS

In this section, we will first discuss the conductivity and the interactions between L-lysine (in brief lysine) and water, in binary aqueous solutions without oleic acid. We will then elucidate interactions between oleic acid and lysine, without water. Finally, we will examine interactions in ternary mixtures of lysine, oleic acid and water, their rheological properties and crystalline structure, as well as their piezoelectric properties. Preliminary data obtained with another amino acid, namely L-arginine (in brief, arginine), are instead provided in the supplemental information file (Figures S9–S11).

Lysine and arginine yield electrically conductive solutions in water, with unadjusted pH, as seen in Figure 1. Without adjustment and with 0.2–0.8 M lysine in water, the pH is approximately equal to 10. Recall that the pKas of the alpha carboxyl and alpha amino groups of lysine are 2.16 and 9.06, respectively, while the pKa of the sidechain amino group is 10.54. For arginine, the pKas of the alpha carboxyl and alpha amino groups are 2.14 and 8.72, respectively, while the pKa of the sidechain amino group is 12.48. Fits of conductivity data for different amounts of lysine added to water using Zhang et al.'s model yield a value of *n* for lysine close to 1, indicating almost complete dissociation of lysine in water, as discussed in the materials and methods section. The lower value of *n* for arginine is consistent with its lower solubility in water. The lower degree of arginine dissociation in water can account for the lower conductivity observed.

The conductivity of amino acids in aqueous solutions was previously reported.[35] The dielectric constants of amino acid mixtures in water have been found to increase with amino acid concentrations ranging from 0.1 mol/kg to 0.35 mol/kg of solution for L-proline, glycine, L-alanine, and L-serine.[36] A study from 1951 reports changes in electrical conductivity during bacterial growth, due to amino acid formation in the growth medium, observed even before bacteria began to multiply.[37] The electrical conductivity of amino acids has been further examined in a study from 1959, which discusses alanine, glycine and tyrosine, as well as proteins (of which amino acids are building blocks).[38] In their native environment, proteins conduct mainly through electron transfer, although they also allow short-range electron transport upon integration into solid-state junctions.[24] While proteins conduct electricity in both their wet and dry states, the electrical conductivity of proteins markedly increases with increasing adsorbed water.[27] Similarly, water layers adsorbed on the surface of a peptide promote proton conduction, and carboxylic acid side chains act as proton-donors, thereby playing an important role for conductivity.[24] Previous authors proposed that the percent humidity affects the conduction mechanisms of peptides (of which amino acids are also building blocks).[39] Specifically, at low relative humidity, conduction is mediated by electrons and protons, whereas at high humidity conduction increases and is mediated by protons.[39] As discussed in the introduction, the pyroelectric and piezoelectric effects are correlated to one another. A study proposes that the pyroelectricity of amino acid crystals is due to layers where the polar moieties of the amino acids are hydrated.[40] The authors report that amino acid crystals were markedly less pyroelectric after they were fully dried.[40] Another recent study also analyzed the role of a protein-water interface in controlling proton conduction across protein-based biopolymers.[41] This study reports that proton transfer in bovine serum albumin fibers requires a hydrogen (H) bond network between amino acids and water molecules.[41] Another study discusses H bonding between amino acids and water, probed through molecular dynamic simulations.[42] This study investigates a number of amino acids, including lysine and arginine. It reports that amino acids can interact with water by either donating or accepting H bonds. H bond donors include the amino groups NH, NH_2, and NH_3 of lysine, arginine and other amino acids. H bond acceptors include the CO carbonyl groups. The OH on the -COOH groups can

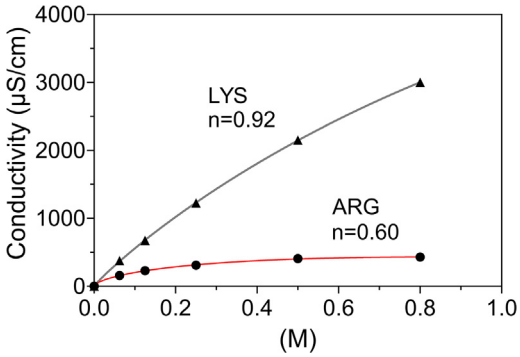

Figure 1. Electrical conductivity of aqueous solutions of lysine (LYS) and arginine (ARG), with varying amino acid molar concentrations

In the figure, the experimental data points are shown as symbols, whereas the continuous lines represent the fit using the model by Zhang et al.[34] Error bars are fairly small. The averages and standard deviations estimated based on three to five measurements are as follows. Pure water: 1.07 ± 0.10 μS/cm. Lysine: 0.0625 M 373 ± 2 μS/cm, 0.125 M 684 ± 19 μS/cm, 0.25 M 1275 ± 32 μS/cm, 0.5 M 2290 ± 78 μS/cm. Arginine: 0.0625 M 167 ± 8 μS/cm, 0.125 M 233 ± 6 μS/cm, 0.25 M 288 ± 10 μS/cm, 0.5 M 411 ± 5 μS/cm.

either accept or donate H bonds.[42] The fact that lysine can either accept or donate H bonds is reflected in its sigma profile, shown in Figure S2 (supplemental information file).

We use ATR-FTIR to probe the interactions between lysine and water, comparing the IR (infra red) spectrum of dry lysine with the spectrum of lysine in water (Figure 2A). In the spectrum of dry lysine shown in Figure 2, in the 1,200–1,800 cm^{-1} region, there are peaks at 1,403 cm^{-1} (ν_s(COO) [43,44]) and at 1,615 cm^{-1} (ν_{as}(COO)), and at 1,582 (ν_{as}(COO) [45] or δ_{as}(NH) +ν_{as}(COO) [46]). There are also peaks at 1,510 cm^{-1} and 1,561 cm^{-1} (δNH_2 [43,47,48]). Rao et al. report that the NH band at higher frequencies (1,560 cm^{-1}) is bonded, whereas the one at lower frequencies is free.[49] Note that other authors ascribe the peak at 1,561 cm^{-1} to non-pure modes due to ν(COO) and δ(NH) vibrations.[50] Moreover, some authors report that lysine can be in a zwitterionic state even in its solid form, not only in aqueous solutions.[51] Others report the co-presence of neutral and zwitterionic forms of other amino acids, including glycine, sarcosine and N,N-dimethylglycine.[52] Therefore, we cannot discount that each of the two NH bands seen in the IR spectrum corresponds to NH_2 and NH_3^+, since the strength of the N-H bond should differ between NH_3^+ and NH_2 groups. This aspect will be further discussed later. In dry lysine, H bonding between lysine molecules occurs through the NH and carboxyl groups. A previous study reports that the crystalline structure of L-lysine is layered and contains two hydrogen-bonded regions.[53] One region is composed of two H bonded sheets, each of which is formed by the head groups two L-lysine molecules: the ammonium groups act as H bond donor and the carboxyl groups act as H-bond acceptor. In the other region H bonding occurs exclusively between NH_2 groups that are connected to each other by the two-one screw axis.[53]

Upon mixing with water, the NH peak at 1,510 cm^{-1} corresponding to free amines markedly decreases, indicating that H bonding between lysine and water occurs through this group. Also, the peak corresponding to bonded NH at 1,561 cm^{-1} shifts to lower wavenumbers. H bonding can affect the peak position, as for instance reported for the NH band of melamine upon H bonding triazine.[54] Moreover, a study reports that protonation induces large red shifts in the ν(NH) wavenumbers.[55] We propose that the NH groups of lysine can form more H bonds when lysine is in water than when it is in the dry form, as indicated by the relative decrease in peak corresponding to free NH. This is likely because the NH groups of lysine become more protonated when lysine is mixed in water, compared to its dry state. Aqueous lysine solutions (with 0.2–0.8 M lysine) have a pH ≈ 10. At this pH, lysine exists in a zwitterionic state with one COO-, one NH_2, and one NH_3^+ group. As aforementioned, we cannot discount that the two amine peaks correspond to NH_2 and NH_3^+. Also, the symmetric stretching vibration ν_s(COO) of lysine at 1,403 cm^{-1} shifts to higher wavenumbers upon mixing with water, suggesting that H bonding of the -COOH group with other molecules is weaker in aqueous lysine solutions than in dry lysine. This could account for the activity coefficients shown in Figure S3 (supplemental information file). These are >1 for both lysine and water in aqueous lysine solutions.

Note that lysine is a basic amino acid, and it can therefore affect H bonding of water directly, by interacting with H_2O, or indirectly, by increasing the proportion of hydroxyl groups in water. A previous study proposes that at acidic pH, protons enhance H bonds only locally.[56] In contrast, at basic pH, hydroxide ions induce tetrahedrality in the H bonding network of water.[56] Therefore, the increased percentage of OH groups induced by lysine should enhance H bonding in water. Direct H bonding between lysine and water would also affect the H bonding network in water. In our previous studies, we used the OH stretch band of water to probe H bonding. Here, we cannot analyze lysine-water interactions through the OH groups using IR, since both water and lysine have a contribution in the OH stretch region (2,500–4,000 cm^{-1}).

For this reason, we analyze solutions of lysine in D_2O, since there is a less marked overlap between ν(DO) and lysine, as seen in Figure 3. Figure 3 also shows data for ternary mixtures containing water, lysine, and oleic acid, which will be discussed later. Deconvolution of the DO stretch band is given in the supplemental information file (Figure S4). The data show that lysine increases the area of peaks at the lowest wavenumbers, compared to those at the highest wavenumbers. A previous study reports that addition of bases such as LiOH or NaOH to D_2O increased the area of the peaks at high wavenumbers relative to low wavenumbers.[57] In contrast, here we observe the opposite effect, i.e., an increased area under peaks at low wavenumbers. We ascribe this result to interactions between lysine and D_2O, rather than to the increase in the OH groups. Shi et al. used mid-IR to probe D_2O at different temperatures, ranging from 10 to 245 K.[58] The IR spectra presented by the authors display a dominant peak at approximately 2,400 cm^{-1} at 10 K (at which D_2O is most crystalline and ordered) and a dominant peak slightly below 2,500 cm^{-1} at 245 K (at which D_2O is least ordered). In our study, the ratio of the peak at approximately 2,407 cm^{-1} and 2,500 cm^{-1} is greatest with lysine in water, lowest for pure D_2O and intermediate between these two cases for D_2O+lysine+oleic acid (Figure 3). We ascribe this result to the fact that lysine structures water. Oleic acid interacts with lysine, thereby limiting its interactions with D_2O and restoring the structure of pure D_2O, as will be further discussed later. H bonding between lysine and water has been previously reported,

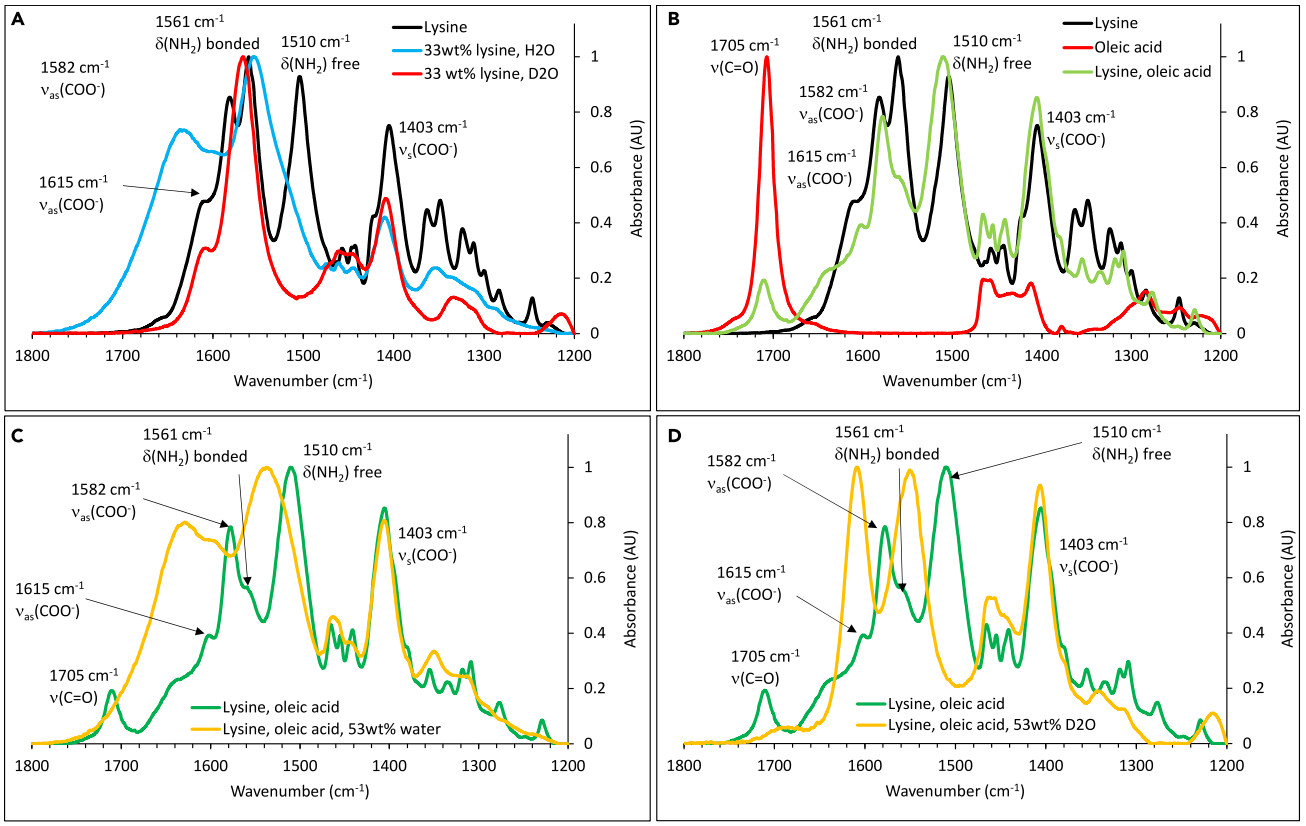

Figure 2. Comparison between the IR spectra in the 1,200–1,800 cm^{-1} region of three types of samples

Dry lysine and of 33 wt % lysine in either water or D_2O (A), dry lysine, oleic acid, and equimolar ratios of oleic acid and lysine (B), equimolar ratios of oleic acid and lysine without water and with 53 wt % water (C), and equimolar ratios of oleic acid and lysine without water and with 53 wt % D_2O (D).

and discussed in the context of the anti-freeze properties of lysine in water.[59] In agreement with this report, our data suggest that lysine creates a more extensive H bonding network in heavy water. This result agrees with the observation that the proportion of H bonded vs. free NH increases in water (although H bonds weaken compared to dry lysine). A caveat when translating observations made with heavy water to understanding solutions prepared with light water is that heavy water is more structured than light water.[60] De Marco et al. proposed that the O–D stretching vibrations of D_2O are qualitatively different molecular vibrations compared to H_2O.[61] Also, carboxylic acids may behave differently in heavy and light water. For example, a study on H bonding of carboxylic acids in water reports peak splitting in the νCC range, which is not observed in H_2O.[62] The authors propose the appearance of a new species in D_2O solution, which is not present in light water.[62] Despite this caveat, overall, our data indicate that lysine can H bond water: H bonding of water becomes more extensive with lysine, and the proportion of NH bonded groups of lysine increases in aqueous solutions (compared to the dry state).

Furthermore, mixing with water markedly shifts to higher wavenumbers the stretching CH bands of lysine, as seen in Figure 4A. Scheiner et al. report *ab initio* quantum calculations showing that CH groups of peptides are strong H bond donors, with binding energies to water molecules equal to 1.9 and 2.5 kcal/mol for nonpolar and polar amino acids, respectively.[63,64] The authors also contend that the H-bond of charged lysine residue of peptides is stronger than a conventional OH··O interaction and induces a blue shift in the CH stretching wavenumber.[63,64]

In addition to interacting with water, lysine interacts with oleic acid. Without water, equimolar ratios of lysine and oleic acid yield a mixture that solidifies over time, to create a hard, brittle material. Figure 4B compares the CH of bands of lysine, oleic acid and their mixtures. Neat oleic acid is not structured and is in the liquid state at room temperature (20°C). This causes the co-presence of trans and gauche conformers, with asymmetric and symmetric deformation modes $\nu_{as}(CH_2)$ at 2,922 cm^{-1} and $\nu_s(CH_2)$ at 2,853 cm^{-1},[65] as seen in Figure 4B. Peaks below 2,920 cm^{-1} for $\nu_{as}(CH_2)$ and 2,850 cm^{-1} for $\nu_s(CH_2)$ are characteristic of a structured state, in which the acyl chains are fully stretched and assume an all-trans conformation. With addition of lysine to oleic acid, $\nu_{as}(CH_2)$ shifts to 2,919 cm^{-1} and $\nu_s(CH_2)$ shifts to 2,850 cm^{-1}, indicating that lysine orders the acyl chains of oleic acid, causing them to acquire a *trans* conformation. Small angle X-Ray scattering (SAXS) data confirm ordering of oleic acid by lysine, as will be discussed later. By interacting with oleic acid, lysine disrupts oleic acid dimers, as indicated by the disappearance of the peak at 935 cm^{-1},[66] as seen in Figure 4D.

Figure 2B shows the COOH and the NH bands of lysine, oleic acid and their equimolar mixtures, without water. The oleic acid carbonyl group can be seen at 1,705 cm^{-1} (ν(C=O)), in Figure 2B. The decrease of this peak to about 10% of its original intensity suggests that the amino

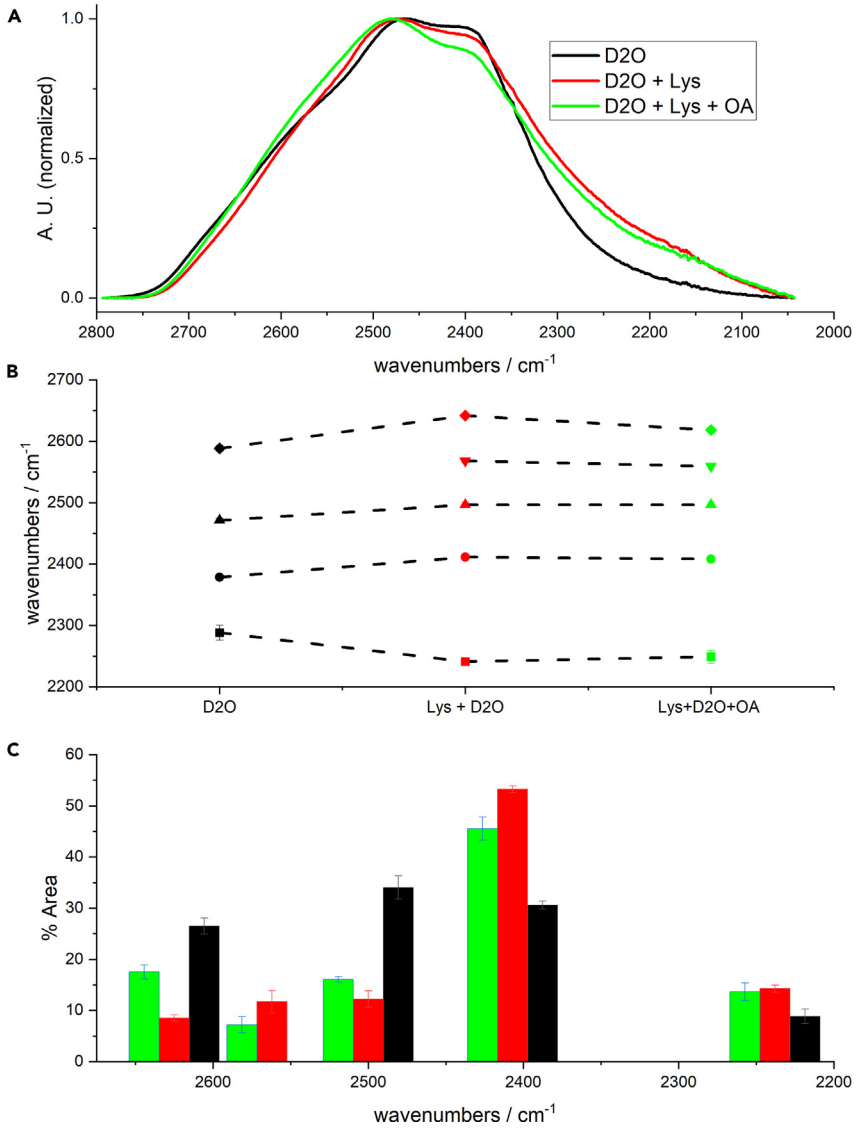

Figure 3. DO stretch band of D_2O

Normalized ν(OH) stretch band (A), peak position (B) and percent area (i.e., proportion, bottom) of the peaks convolved under the ν(OH) stretch band, at different wavenumbers (C).

Since error bars are small and hardly visible in (B), we are providing the data in Table S1 of the supplemental information file.

groups in lysine deprotonate most of the COOH groups in oleic acid, forming the anionic species COO^-. We also observe a marked decrease of the peak at 1,561 cm^{-1}, which almost disappears, relative to the peak at 1,510 cm^{-1}. Earlier in this paper we attributed the peak at 1,561 cm^{-1} to δ(NH_2) of bonded NH groups, and the peak at 1,510 cm^{-1} to δ(NH_2) of free NH groups. It is possible that when combining equimolar ratios of lysine and oleic acid, only one amine group becomes involved in lysine-oleic acid interactions (by interacting with the carboxylic group of oleic acid), while the other amine group remains free. Other interpretations cannot be discounted. As mentioned earlier, some authors ascribe the peak at 1,561 cm^{-1} to non-pure modes due to ν(COO^-) and δ(NH) vibrations,[50] and other authors attribute the peak at 1,510 cm^{-1} to asymmetric CN vibrations.[67] Moreover, we cannot discount that each of the two NH bands corresponds to neutral and protonated NH groups. In particular, we observe that the intensity of the band at 1,561 cm^{-1} decreases, suggesting that it could correspond to the NH_2 vibration. At the same time, the relative intensity of the 1,510 cm^{-1} decreases, suggesting that it may correspond to the NH_3^+ band.

So far, we discussed binary mixtures and interactions between lysine and water, and between lysine and oleic acid (without water). Figure 2 also shows IR spectra of equimolar mixtures of oleic acid and lysine, with water. While lysine solutions in water have a pH of approximately 10, gels containing equimolar ratios of oleic acid and lysine have a circum-neutral pH (pH ≈ 7.5). Upon mixing lysine with both

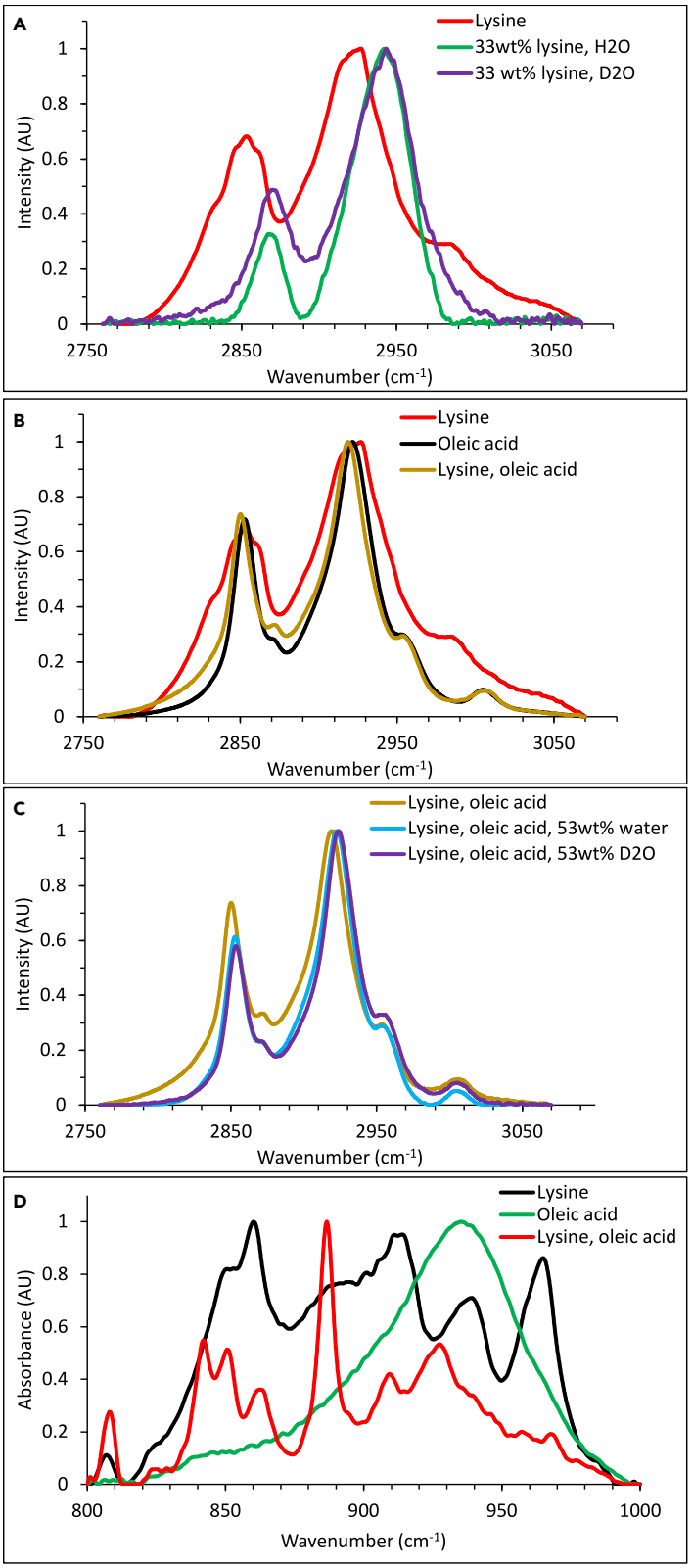
A
Lysine
33wt% lysine, H2O
33 wt% lysine, D2O
Intensity (AU)
Wavenumber (cm-1)
B
Lysine
Oleic acid
Lysine, oleic acid
Intensity (AU)
Wavenumber (cm-1)
C
Lysine, oleic acid
Lysine, oleic acid, 53wt% water
Lysine, oleic acid, 53wt% D2O
Intensity (AU)
Wavenumber (cm-1)
D
Lysine
Oleic acid
Lysine, oleic acid
Absorbance (AU)
Wavenumber (cm-1)

Figure 4. IR spectra in the 2,750–3,100 cm^{-1} region and in the 800–1,000 cm^{-1}

Comparison between the IR spectra in the 2,750–3,100 cm^{-1} region of: dry lysine, and 33 wt % lysine in either water or D_2O (A), dry lysine, oleic acid and their equimolar mixtures without water (B), and equimolar ratios of oleic acid and lysine, without water and with either 53 wt % water or D_2O (C). Comparison between the IR spectra in the 800–1,000 cm^{-1} region of dry lysine, oleic acid and their equimolar mixtures without water (D).

oleic acid and water, the peak at 1,561 cm^{-1} (H bonded NH) increases relative to the one at 1,510 cm^{-1} (free NH) compared to dry lysine, although to a lesser extent than in lysine-water solutions without oleic acid. This result agrees with the hypothesis presented earlier that oleic acid interacts with lysine, thereby limiting lysine-water interactions. This would result in a less extensive H bonding network in water. Furthermore, we observe a difference between the distortion of the ν(OD) band of lysine+D_2O compared to lysine+oleic acid+D_2O, as seen in Figure 3. Recall that this band can be used to study H bonding because it does not overlap with bands contributed by neat oleic acid or lysine (dissimilar to the OH stretch band of water). With lysine and water (without oleic acid), the ν(OD) band has greater contributions from the peaks at the lowest wavenumbers, compared to pure D_2O, as seen in Figure 3 and discussed earlier. Also, the peak at ≈2,400 cm^{-1} (at which D_2O is most crystalline and ordered) increases relative to the peak at 2,500 cm^{-1} (at which D_2O is least ordered), as previously discussed. Oleic acid restores the relative proportion of the peaks convolved under the ν(OD) band. Once again, we propose that oleic acid interacts with the NH groups of lysine, thereby limiting water-lysine interactions and decreasing D_2O ordering. Finally, there is essentially no frequency shift in the acyl chain peaks at 2,900 cm^{-1} upon the addition of water or D_2O to oleic acid-lysine mixtures (Figure 4). However, these bands are narrower (particularly the $\nu_{as}(CH_2)$) with water compared to no water. It is possible that addition of water limits hydrophobic interactions of lysine with the acyl chains of oleic acid, creating a less diverse molecular environment. Indeed, the CH groups of lysine significantly interact with water, as discussed earlier. Hydrophobic interactions have been reported to play a role in the overall interaction between poly-L-lysine and the negatively charged phospholipid dipalmitoyl phosphatidyl glycerol.[68] This would also reflect on the ordering of the oleic acid chains. The structure of oleic acid-lysine mixtures with and without water was examined by SAXS (small angle X ray scattering), as discussed later.

While equimolar mixtures of lysine and oleic acid are hard and brittle, gels are obtained with 85–90 wt % water and equimolar ratios of oleic acid and lysine. Figure 5 shows strain and frequency sweeps conducted in shear rheology experiments. The storage moduli (G′) are greater than the loss moduli (G″) between frequencies of 0.1–100 rad/s. Specifically, tanδ = G″/G′ is 0.15 and 0.31 with 85 wt % and 90 wt % water, respectively, demonstrating that the materials obtained are gels. As mentioned earlier and discussed in the supplemental information file, arginine also yields gels. Both lysine and arginine are linear molecules and have electrically charged side chains. Histidine contains a ring and it yields emulsions rather than gels upon mixing with oleic acid and water. Also, L-serine, L-threonine, and D-alanine do not yield gels. Also note that while gels are obtained with lysine and arginine, oleic acid, and pure water, addition of salts (e.g., 0.2 M NaCl) disrupts the gels (cf. Figure S5, supplemental information file). This result demonstrates the fact that electrostatic interactions between lysine and oleic acid (such as H bonding) play a key role. Without salts, gels were stable over a period of three weeks, both at room temperature (≈20°C) and in the fridge (4°C). Longer observations were not conducted. During this time and at these temperatures, we did not observe any changes when gels were prepared with deionized or Milli-Q water. In contrast, gels could not withstand exposure to −80°C for 48 h. When they were exposed to −80°C and thawed, they were liquid rather than gels.

Figure 6 compares polarized light microscopy images of equimolar oleic acid-lysine mixtures without water and with water. Polarized light microscopy reveals that water fosters the formation of structures spanning hundreds of microns, which extend across the gel. Without water, such large structures are not observed. We hypothesize that the elasticity of the materials is due to these structures.

A previous study reports that the crystal structure of neat L-lysine is layered and contains two hydrogen-bonded regions.[53] The authors assign the hydrogen-bonded sheets in the crystal structure of L-lysine to the L2 structure type.[53] Note that an older study also analyzed the crystalline structure of L-lysine and reports a monoclinic structure, a primitive $P2_1$ space group, with a = 4.902 Å, b = 30.719 Å, and c = 9.679 Å, β = 90º, and V = 1457.7 $Å^3$.[69] In our previous study, we determined that oleic acid at 4°C self-assembles into lamellar structures.[1] Here, we use synchrotron SAXS (small angle X ray scattering) to characterize the structure of the lysine-oleic acid mixtures, in the presence and in the absence of water, as well as in the absence and in the presence of applied electric fields (Figures 7, 8, and 9). SAXS data show that equimolar ratios of lysine and oleic acid yield lamellar structures with a d spacing, d = 55.3 Å, in the absence of water or applied electric fields. Considering that the size of an oleic acid crystalline lamella from our X-ray diffraction (XRD) data is 41.6 Å and the size of a lysine crystalline lamella is 16.2 Å (Figure S6 and a study by Pensini et al.[1]), and the size of a crystalline lysine-oleic acid lamellar complex is 55.3 Å, we propose that the structure of this complex is composed of two oleic acid and two lysine molecules (Figure S7, supplemental information file). With water (54–85 wt %) and without electric fields, equimolar oleic acid-lysine mixtures acquire a columnar, hexagonal crystal structure, as seen from the peak positions shown in Figure 8 ($1 : \sqrt{3} : \sqrt{4} : \sqrt{7}$; study by Hyde[70]). Water swells the structures formed, increasing their size from approximately 61 Å with 45 wt % water to 115 Å with 85 wt % water, at an equimolar lysine to oleic acid ratio. Note that hexagonal mesophases can arrange to form ribbons,[70] which we observed in other piezoelectric gels obtained with oleic acid and ethanolamine.[1] Further increasing the water content to 89 wt % yields another transformation from hexagonal crystals to bi-continuous cubic sponges, in the absence of applied electric fields (Figure 8).

SAXS also reveals that electric fields change the crystalline structure of gels of lysine, oleic acid and water, as demonstrated for samples containing 89 wt % water (Figure 8). These undergo a crystalline phase transition from a bi-continuous cubic sponge to a lamellar structure upon applying 1 V. The transformation is progressive, as seen by applying a voltage ramp (with 0.2 V increments). The observed changes are due to the piezoelectric nature of the materials developed, as shown by cyclic voltammetry, and as will be further discussed later. A study applied very high electric fields (up to $4.0 \cdot 10^6$ V/cm) to unoriented and biaxially oriented phase-II poly(vinylidene fluoride) films.[71] This study

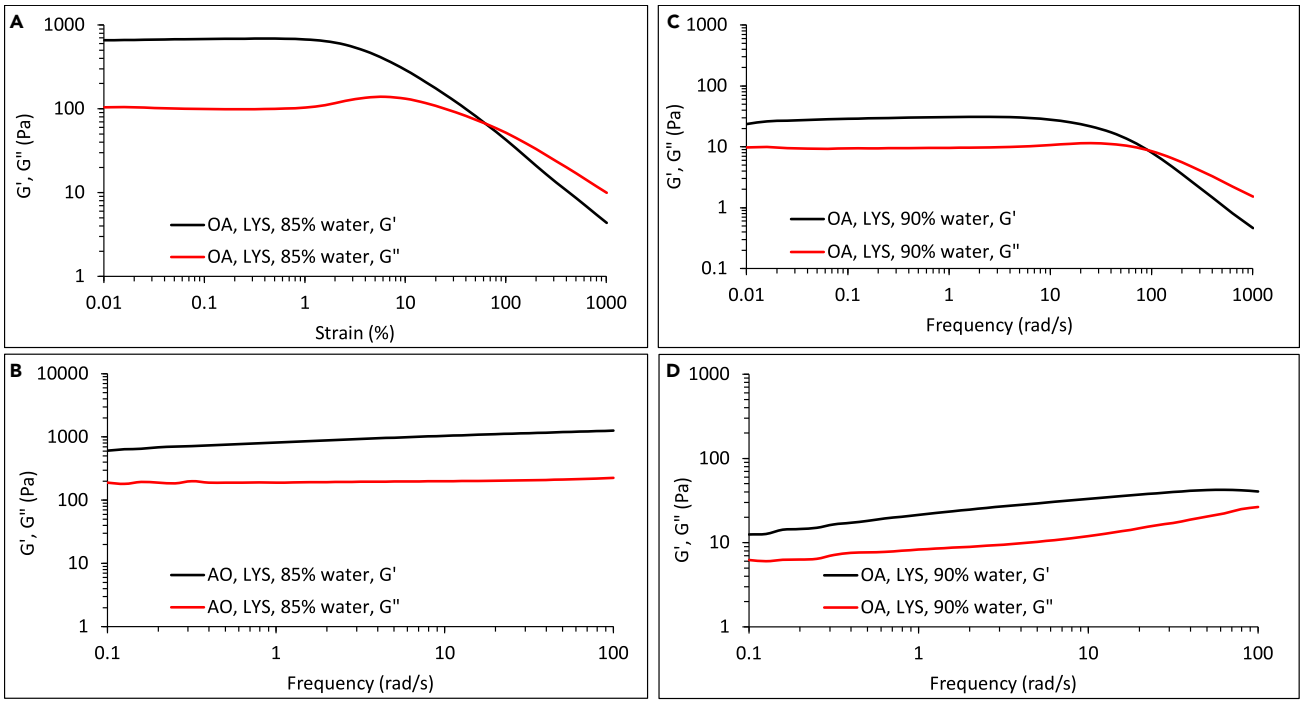

Figure 5. Shear rheology strain and frequency sweeps

Strain (A and C) and frequency sweeps (B and D) of gels obtained with lysine, oleic acid and either 85 wt % water or 90 wt % water.

found that the applied electric field induced both a crystal transformation and an increase of the piezoelectric activity.[71] More recently, a density functional theory study showed that applied electric fields caused a transition from α to β chains of poly(vinylidene fluoride).[72] Other authors also report that lead zinc niobate-lead titanate single crystals undergo very large piezoelectric strains when electric fields are applied

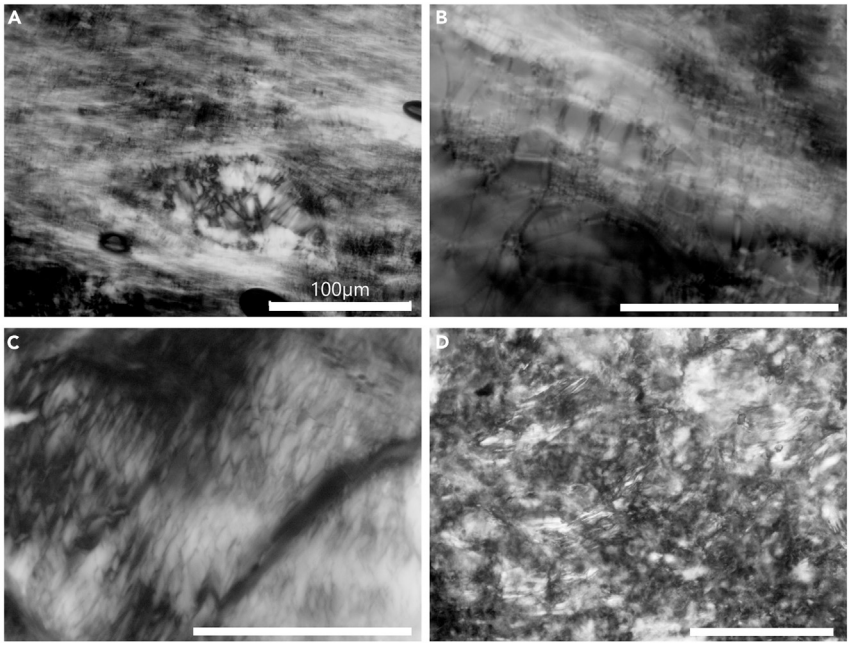

Figure 6. Polarized light microscopy of piezoelectric materials

Polarized light microscopy of materials obtained with equimolar ratios of lysine and oleic acid, with 75wt % water (A, B, and C) and without water (D). The scale bar is 100 μm.

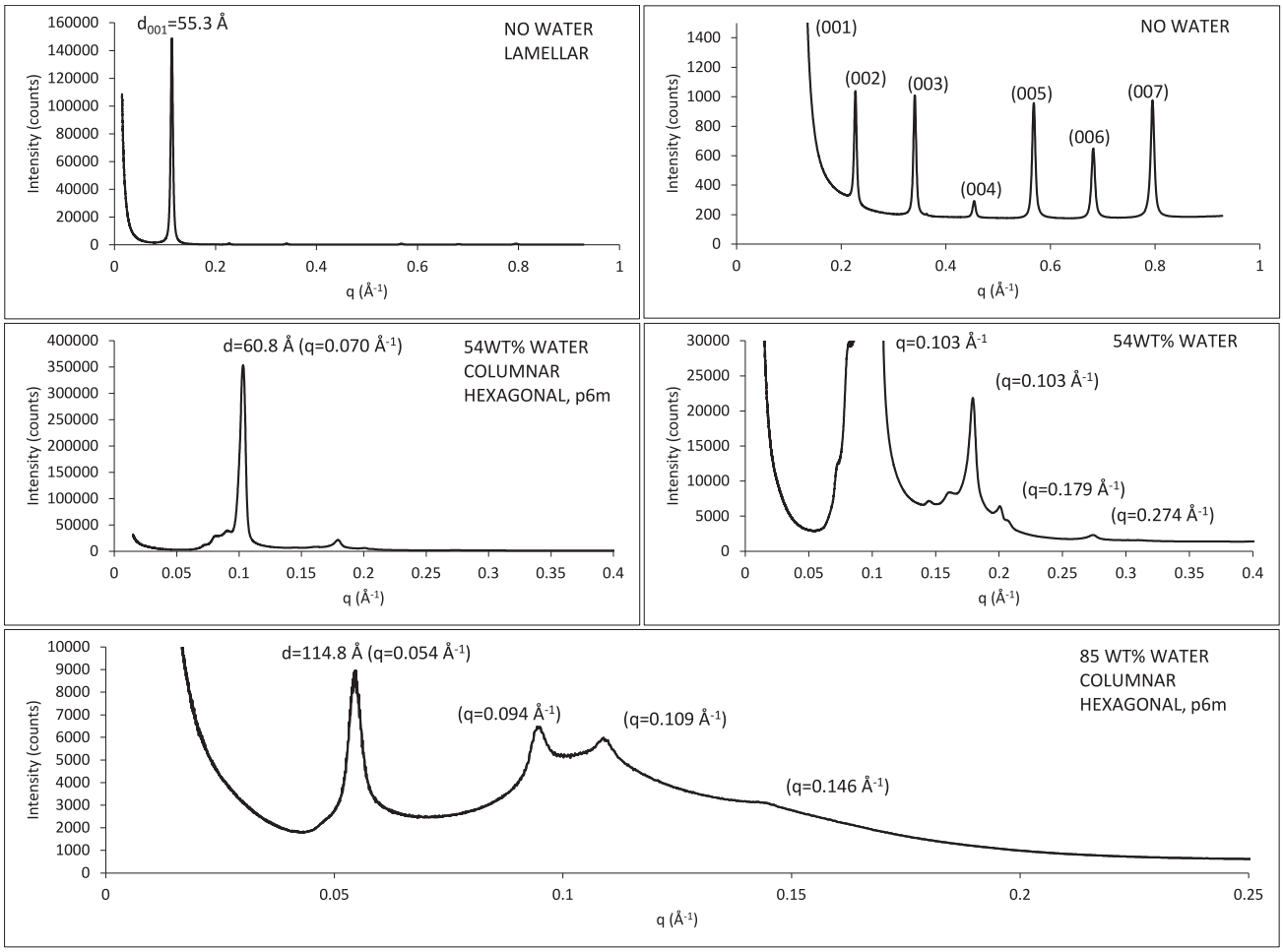

Figure 7. Synchrotron SAXS patterns of equimolar mixtures of oleic acid and lysine, without water and with varying water percentages

along the unit cell edges.[73,74] Park et al. propose that this is due to a phase transition,[74] whereas Kisi et al. contend that a phase transition is in this case indistinguishable from a large piezoelectric distortion.[73]

The effect of electric fields is further highlighted by applying 10–20 V to samples containing equimolar ratios of lysine and oleic acid, and 89 wt % water. We determined the azimuthal plots for these samples, as well as for samples without applied electric fields, as shown in Figure 10. Azimuthal plots show intensity variations relative to the average for different azimuthal angles. The fitting parameters are given in the supplemental information file (Tables S2–S4). The variations of the intensity seen in the azimuthal plots are related to orientation in the sample. Without any applied voltage, samples display some orientation. This orientation is markedly accentuated upon applying 10 V to the samples, as indicated by the evident increase in the integrated intensity peaks shown in Figure 10A. Also, with 10 V ordering increases, as seen by the decreased peak width (characterized by the full width at half maximum, fwhm). The standard deviation of the Gaussian curves used to fit experimental data is ≈ 17.5 without applied voltage and 16 with 10 V. Interestingly, 20 V decrease ordering and increasing the standard deviation of the Gaussian curves to ≈22. Nonetheless, the azimuthal plot of the normalized integrated intensity (Figure 10B) reveals a progressive shift of the intensity peaks from 0 V, to 10 V and finally to 20 V. This shows that the applied electric field progressively aligned the crystalline structures within the sample. Note that while this effect was most marked at these high voltages, a similar effect was also seen in voltage ramps conducted with 0.2 V increments, up to 1 V. In particular, the position of the intensity peaks progressively shifted, indicating once again that the applied electric fields aligned the structures in the sample, as seen in Figure S6 (supplemental information file). Nonetheless, the applied voltage ramp up to 1 V did not increase orientational ordering, as indicated by the progressive increase in peak width (Table S5, supplemental information file). We explain these results based on the relative orientation of the applied electric field relative to the initial orientation of the crystalline structure in the sample. This was largely random, as samples were in part compressed upon mounting in the SAXS sample holder. The data show that applied fields aligned the structures in the sample. Nonetheless, if the direction of the applied field was at an angle relative to the initial orientation of the structures in the samples, disorder could increase within the time frame during which experiments were conducted. Note that a widening of the Gaussian peaks could have also been due to an increase in temperature during the course of the measurements, although temperature was not monitored.

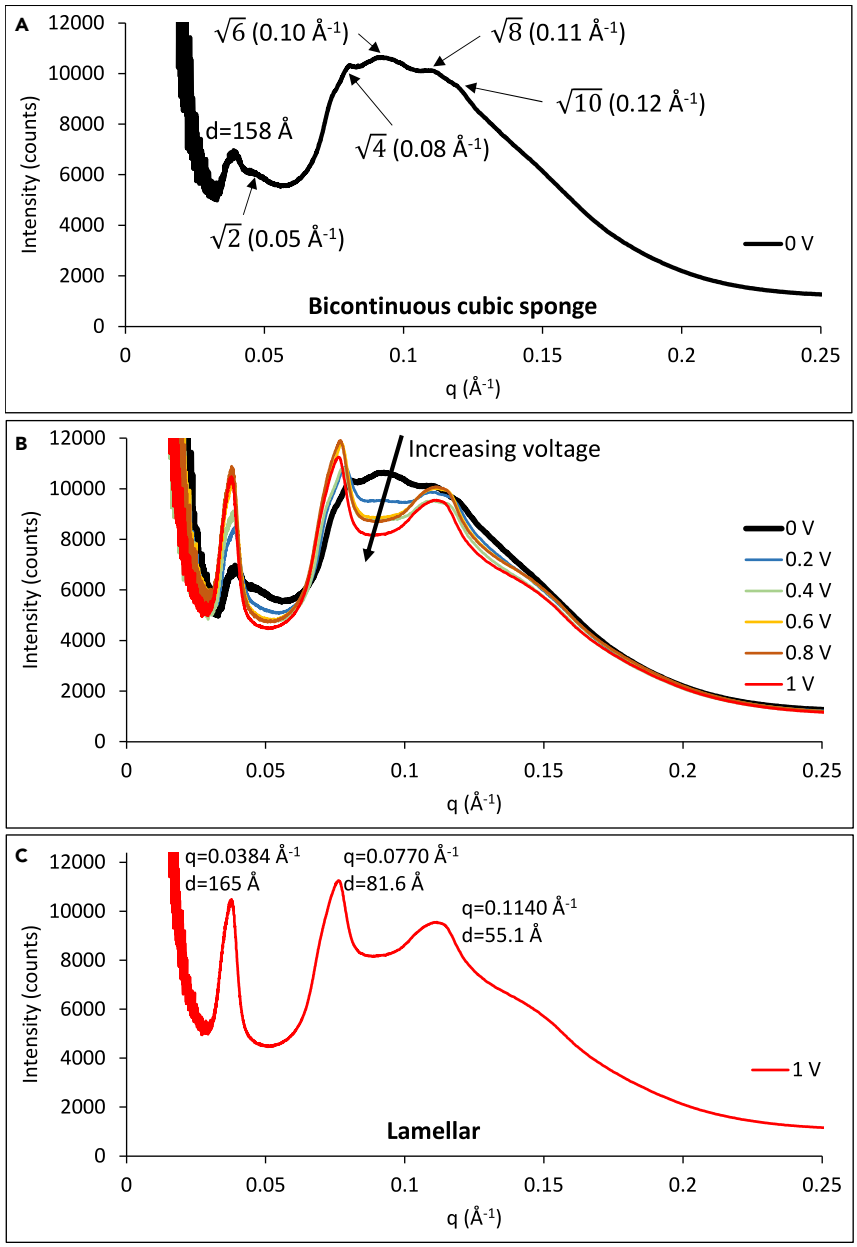

Figure 8. SAXS pattern of a sample containing equimolar ratios of oleic acid to lysine and 89 wt % water

SAXS pattern of a sample containing equimolar ratios of oleic acid to lysine and 89 wt % water, without electric fields applied (A); comparison between the SAXS patterns of this sample before and after applying voltages increasing from 0 to 1 V, in increments of 0.2 V (B); SAXS pattern for the sample upon exposure to 1 V (C).

In addition to SAXS, XRD was used to analyze oleic acid-lysine mixtures, as shown in Figure S7 (supplemental information file). The data confirm that the pattern of oleic acid+lysine mixtures is not merely the overlap of the XRD peaks observed with neat oleic acid and neat lysine. The data also reveal that water impacts the crystalline structure of oleic acid-lysine mixtures, rendering them more amorphous in the WAXS (wide angle X ray scattering) region at the highest water percentages tested (75 wt %).

Note that here we have not investigated the effect of oleic acid to lysine ratio on the crystal structure of their mixtures, nor have we systematically examined the effect of fatty acid chain characteristics. Both would affect the crystal structure, thereby impacting the piezoelectric properties of the materials. For example, the structures observed here with oleic acid (unsaturated) differ from those reported for saturated fatty acids, lysine and water mixtures.[75] With saturated fatty acids, the authors observed aggregates ranging from micelles, vesicles, sponge structures, and fibers depending on the composition and the chain length of fatty acids.[75] A systematic investigation of the

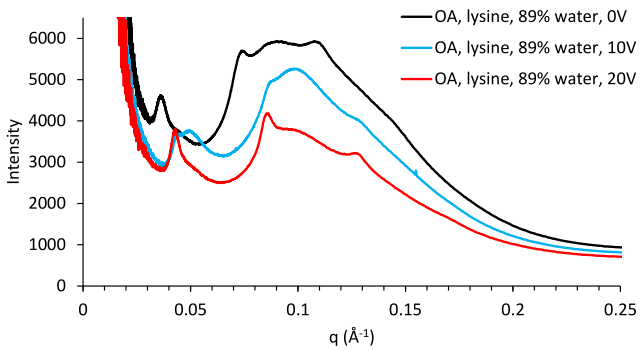

Figure 9. SAXS pattern of a sample containing equimolar ratios of oleic acid to lysine and 89 wt % water, without electric fields applied, and upon applying 10 V and 20 V

fatty acid characteristics and fatty acid to amino acid ratio on the crystal structure and piezoelectric behavior of the materials developed will be the objective of our future research. Although we have not conducted such a systematic investigation, we also probed the structure of materials obtained with lysine and linoleic acid, using SAXS and XRD. SAXS data also reveal lamellar structures upon mixing equimolar ratios of linoleic acid and lysine, without water (supplemental information file, Figure S9). Instead, SAXS patterns were amorphous with 85 wt % water (supplemental information file, Figure S10). In this research, we used SAXS, XRD, and polarized light microscopy to characterize the piezoelectric gel structures. Atomic force microscopy and transmission electron microscopy may also provide useful insights in future research.

Cyclic voltammetry experiments conducted by the method described previously demonstrates that materials obtained with equimolar ratios of oleic acid, lysine and 74–85 wt % water show significant double layer charging in the region examined, which would be expected for a piezoelectric material (Figure 11). This is evident from the shape of the cyclic voltammetry curves, which show that electricity is not zero at the origin. Using the cyclic voltammetry curves taken at different scan rates we estimate an anodic capacitance of 0.7–0.9 mF/cm^2 and a cathodic capacitance of approximately 0.6–0.7 mF/cm^2.

The human blood contains 83% water, the heart 79%, and the brain 73%. Note the similarity between the water content of the piezoelectric materials developed and the water content of different human organs and blood. Given this similarity and the gel composition, we expect that

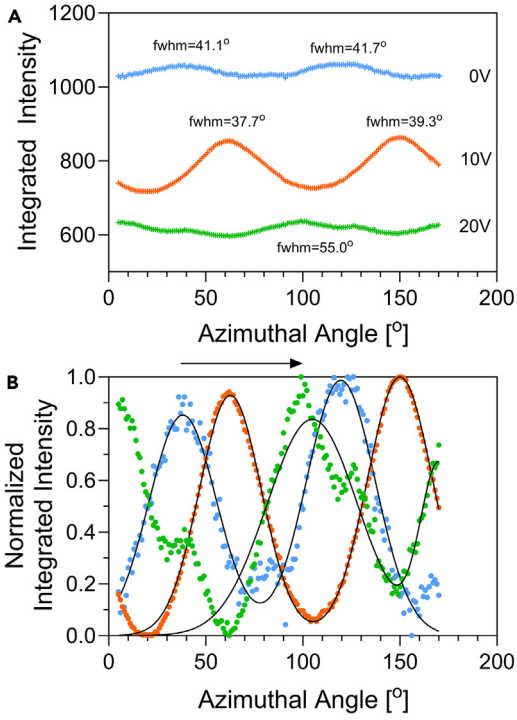

Figure 10. Azimuthal plot for piezoelectric materials containing lysine, oleic acid and 91wt% water

Azimuthal plot showing the integrated intensity (A) and normalized integrated intensity (B) of SAXS patterns over different azimuthal angles.

Samples contained equimolar ratios of lysine and oleic acid, and 91 wt % water. These plots compare samples without applied electric fields, and upon applying either 10 V or 20 V. In (B), the colored symbols are the experimental data and the continuous black lines are the fits to the data. The fwhm was calculated from the standard deviation SD of the Gaussian peak, as fwhm = 2.355·SD.

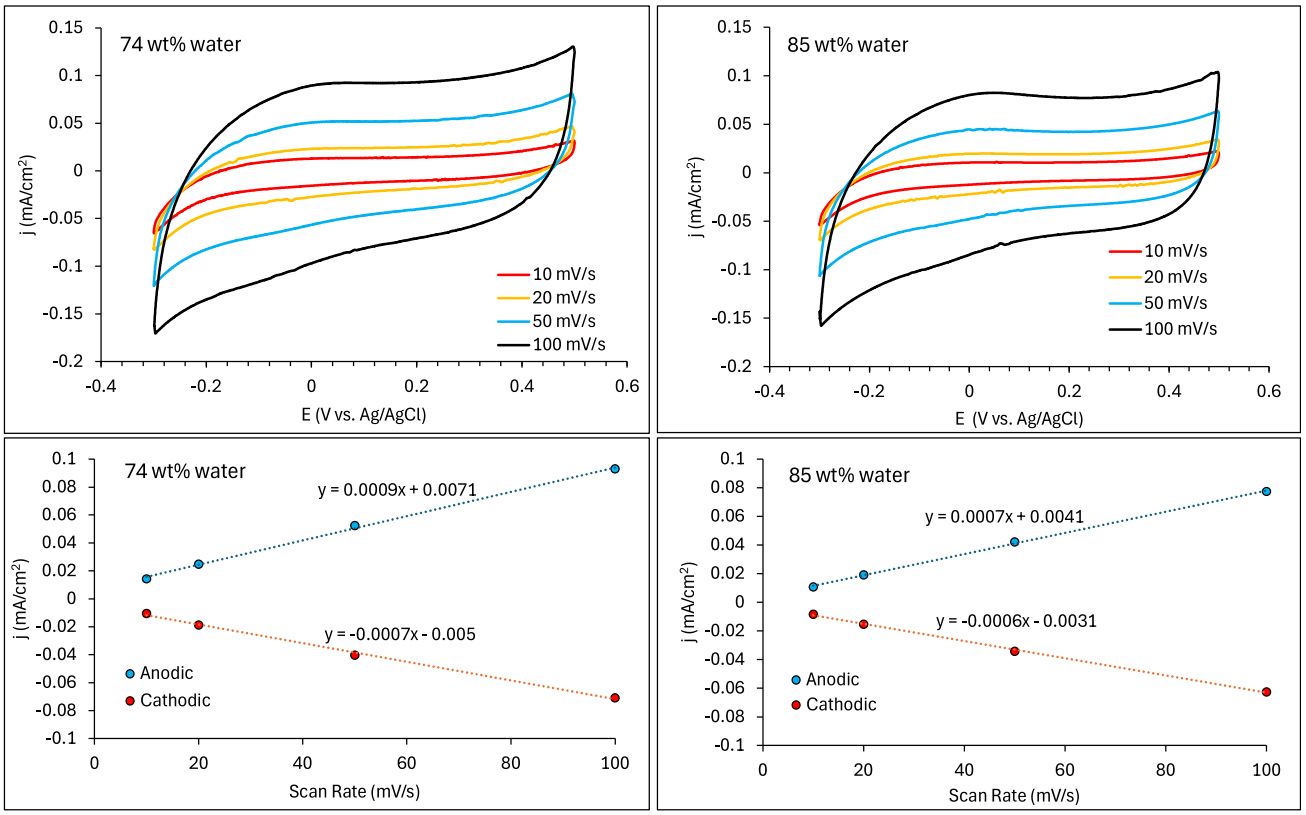

Figure 11. Cyclic voltammetry curves (current j vs. voltage E, normalized by the area of the electrode) obtained using a graphite working electrode, using materials obtained with equimolar ratios of lysine and oleic acid, and water (74 and 85 wt %), and current vs. scan rate

The current values were taken at a voltage of 0.2 V. Note the error bars in the figure are small (<0.002) and thus not visible.

our piezoelectric materials have significant potential for medical applications. Fatty acids are the building blocks of cell membranes and amino acids are the building blocks of proteins, and they are the constituents of our gels.

Given their piezoelectric nature, the volume of materials containing equimolar ratios of lysine and oleic acid, and 91 wt % water deform and change volume when exposed to an electric field, as seen in Figures 12 and 13. The piezoelectric coefficient measures the volume change occurring when a piezoelectric material is subjected to an electric field.[76] In the samples tested, the volume change was 18% (from 7 to 5.7 mm^3) when materials containing equimolar ratios of lysine and oleic acid, and 91 wt % water were exposed to 5 V for 17 s, using steel wire. This voltage corresponds to 3,626 V/m, based on the electrode distance. If equilibrium had been reached after 17 s, this volume change would have corresponded to a piezoelectric coefficient of 3.6×10^{-13} m/V. However, equilibrium is not immediately reached, as seen in Figure 13. After more extensive exposure of the material to higher voltages (up to 10 V), we estimate a piezoelectric coefficient of approximately $1.2 \cdot 10^{-13}$ m/V. Note that these values are approximate, because of the numerous air pockets, which were not taken into account in the estimate of the volume in the measurement shown in Figure 13. As a reference, the piezoelectric coefficient for quartz is $2.3 \cdot 10^{-12}$ m/V, while the piezoelectric coefficient for barium titanate is $1–1.9 \cdot 10^{-12}$ m/V.[76]

In summary, lysine and oleic acid yield piezoelectric crystalline gels upon mixing with high proportions of water. The crystalline structure of these materials can be tuned by applying electric fields, as a result of their piezoelectric nature.

While this manuscript mainly focuses on lysine, the amino acid arginine also yields piezoelectric gels. Preliminary data obtained with arginine are enclosed in the supplemental information file (Figures S10–S13). Arginine yields conductive solutions in water, although the conductivity is lower than for lysine, as seen in Figure 1. Dissimilar to lysine, arginine yield dispersions in oleic acid, which phase separate over time. While arginine and oleic acid remain phase separated without water, they yield gels in the presence of water. The storage moduli (G′) are greater than the loss moduli (G″) between frequencies of 0.1–100 rad/s. Specifically, tanδ = G′/G′ is 0.21 and 0.31 with 85 wt % and 90 wt % water, respectively (Figure S10). Cyclic voltammetry also show some differences in the piezoelectric behavior with arginine than lysine (compare Figures 11 and S13, supplemental information file). With arginine, oleic acid and 85 wt % water, the anodic capacitance is 0.6 mF/cm^2, and the cathodic capacitance is 0.5 mF/cm^2. Arginine has more NH groups compared to lysine and these groups would interact with the carboxyl groups of oleic acid. Our future research will focus on further exploring the piezoelectric properties of hydrogels obtained with fatty acids and benign molecules containing amine groups, to obtain materials useful for clean energy production, medical patches to promote healing or sensors.

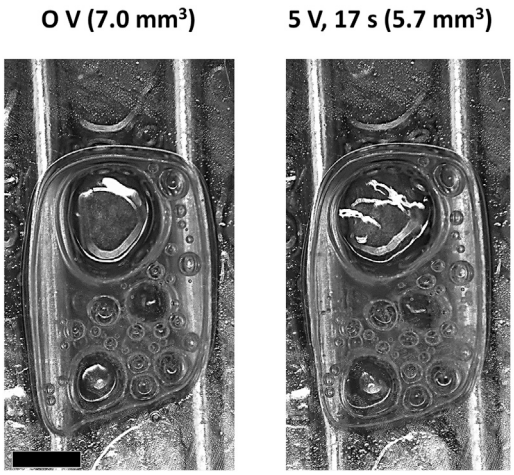

Figure 12. Contraction from 7 to 5.7 mm^3 of a material containing equimolar ratios of lysine and oleic acid, and 91 wt %, upon applying 5 V for 17 s, using a steel wire

The scale bar is 1 mm. The material was confined in a cell 1 mm thick, without constraining its sides. Note that only the largest air pockets were subtracted from the overall volume to obtain the actual volume occupied by the soft piezoelectric material.

DISCUSSION

This study describes piezoelectric hydrogels containing large percentages of water (up to 89 wt %), and equimolar ratios of oleic acid and either lysine or arginine.

Lysine yields conductive solutions in water. Conductivity vs. lysine concentration curves are well described by the model by Zhang et al. Based on the parameters estimated by fitting the model to the data, we conclude that lysine is largely dissociated in water. Arginine also yields conductive solutions in water, but its dissociation is lower, thereby resulting in lower conductivity.

ATR-FTIR demonstrates H bonding between lysine and water. In addition to NH and COOH groups, CH groups also interact strongly with water, as indicated by the marked blue shift of the CH stretch band. H bonding is further revealed by analyzing the DO stretch band of D_2O, which does not overlap with bands contributed by lysine. Lysine-D_2O interactions result in a distortion of the DO stretch peak, increasing contribution from peaks at low wavenumbers. This is indicative of the ability of lysine to structure D_2O, due to H bonding.

Lysine also interacts with oleic acid (at equimolar ratios), yielding a brittle solid with a lamellar crystalline structure, as shown by synchrotron SAXS. With 54–85 wt % water, oleic acid-lysine equimolar mixtures acquire a columnar, hexagonal crystalline structure, while they form bi-continuous sponges with 89 wt % water. Shear rheology demonstrates that these materials are hydrogels between frequencies 1–100 rad/s (i.e., their elastic modulus G′ exceeds their viscous modulus G″). Specifically, tanδ = G″/G′ is 0.15 and 0.31 with 85 wt % and

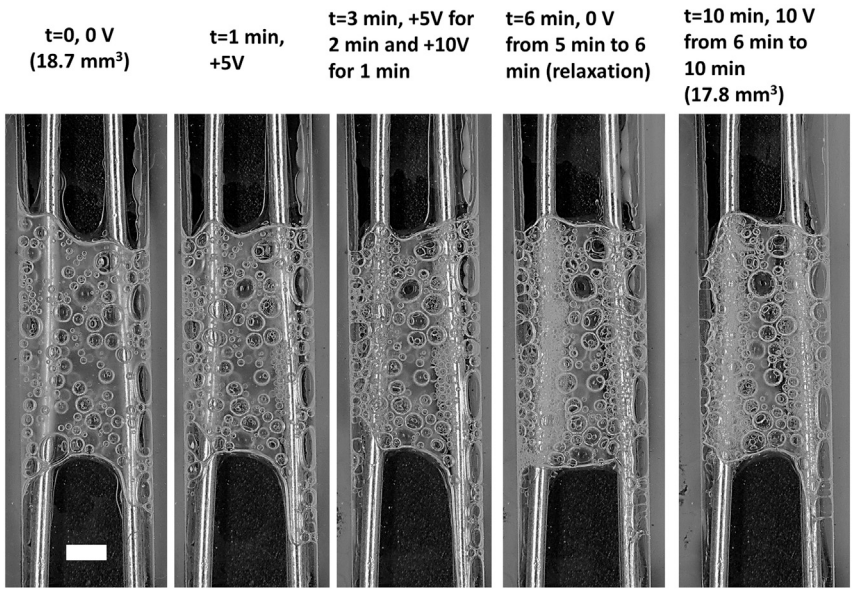

Figure 13. Contraction from 18.7 to 17.8 mm^3 of a material containing equimolar ratios of lysine and oleic acid, and 91 wt %, using a steel wire

The material was confined in a glass cell, 1 mm thick and roughly 3 mm wide. The scale bar is 1 mm. Note that air pockets were not subtracted from the overall volume to obtain the actual volume occupied by the soft piezoelectric material.

90 wt % water, respectively. Polarized light microscopy reveals self-assembled structures spanning hundreds of microns in size. Such structures are not observed without water.

Applied electric fields (up to 1 V) markedly alter the hydrogel crystal structure. Synchrotron SAXS was conducted on hydrogels with 89 wt % water while exposing them to up to 1 V, allowing us to observe in real time the progressive crystalline phase transition from a bi-continuous sponge to a lamellar structure. We also analyzed samples exposed to 10 V and 20 V. Azimuthal plots of the normalized integrated intensity reveal a progressive shift of the intensity peaks from 0 V, to 10 V and finally to 20 V. This shows that the applied electric field progressively aligned the crystalline structures within the sample.

This effect is due to the piezoelectric nature of the hydrogels, which is revealed by cyclic voltammetry. We estimate an anodic capacitance of 1 mF/cm^2 and a cathodic capacitance of approximately 0.4–0.5 mF/cm^2. When an electric field is applied, hydrogels deform and change volume, as seen by observing them in real time under an optical microscope.

This study mainly focuses on lysine, but arginine mixtures with oleic acid and water are also piezoelectric gels. Arginine and lysine are both endowed with charged side chains, and they are linear. Other amino acids such as histidine L-serine, L-threonine, and D-alanine did not yield gels, demonstrating that both the amino acid structure and charge play a key role.

Limitations of the study

This study has analyzed only a sub-set of amino acids and fatty acids. Our future research will continue examining the correlation between structure of suitable amphiphiles, amino acids or amines and fatty acids and piezoelectric hydrogel performance. The overarching goal of this research is the development of benign hydrogels containing high proportions of water, for diverse applications, ranging from delocalized clean energy production to medical patches that promote healing. We have yet to test the piezoelectric hydrogels developed for these applications.

STAR★METHODS

Detailed methods are provided in the online version of this paper and include the following:

- KEY RESOURCES TABLE
- RESOURCE AVAILABILITY
  - Lead contact
  - Materials availability
  - Data and code availability
- EXPERIMENTAL MODEL AND STUDY PARTICIPANT DETAILS
- METHOD DETAILS
  - Attenuated total reflectance- Fourier transform infrared spectroscopy (ATR-FTIR)
  - Conductivity measurements of mixtures of amino acids in water
  - Cyclic voltammetry experiments
  - Shear rheology and viscosity measurements
  - Powder X-ray diffraction
  - Polarized light microscopy
  - Synchrotron based small angle X-Ray scattering
  - Modeling of conductivity data
  - Estimate of piezoelectric coefficients
- QUANTIFICATION AND STATISTICAL ANALYSIS

SUPPLEMENTAL INFORMATION

Supplemental information can be found online at https://doi.org/10.1016/j.isci.2024.110601.

ACKNOWLEDGMENTS

Part of the research described in this paper was performed at the Canadian Light Source, a national research facility of the University of Saskatchewan, which is supported by the Canada Foundation for Innovation (CFI), the Natural Sciences and Engineering Research Council of Canada (NSERC), the National Research Council (NRC), the Canadian Institutes of Health Research (CIHR), the Government of Saskatchewan, and the University of Saskatchewan. The authors acknowledge the support of the Natural Sciences and Engineering Research Council of Canada (provided through an NSERC Discovery grant, awarded to Dr. Erica Pensini, PIN 537871). The authors thank David Pink and Erszebet Szabo for the helpful discussions, and Adam Leontowich at the Canadian Light Source for his help during the measurements.

AUTHOR CONTRIBUTIONS

E.P. conceived the study. E.P., A.G.M., A.C., and J.v.d.Z. designed the experiments. E.P., J.v.d.Z., P.M., N.K., S.G., and S.M.G. performed the experiments. E.P. and A.G.M. analyzed SAXS data. E.P. and T.L. analyzed ATR-FTIR data. A.G.M. analyzed electrical conductivity data. J.v.d.Z.

analyzed cyclic voltammetry data. E.P. analyzed shear rheology data. E.P. wrote the manuscript. All authors revised and approved the final manuscript.

DECLARATION OF INTERESTS

The authors declare no competing interests.

DECLARATION OF GENERATIVE AI AND AI-ASSISTED TECHNOLOGIES IN THE WRITING PROCESS

AI was not used to assist in writing this manuscript.

Received: May 17, 2024
Revised: July 10, 2024
Accepted: July 25, 2024
Published: July 27, 2024

REFERENCES

1. Pensini, E., Gregori, S., Marangoni, A.G., Mirzaee Ghazani, S., Su, Z., Chen, A., and Kashlan, N. (2024). Ethanolamine piezoelectric hydrogels structured by oleic acid lamellae. J. Mol. Liq. *397*, 124185.
2. Schmidt, J.G. (1707). Curiöse Speculationes Bey Schalflosen Nächten (Chemnitz and Leipzig).
3. Sidney, B.L. (1974). Sourcebook of Pyroelectricity (CRC press).
4. Ha, K.H., Li, Z., Kim, S., Huh, H., Wang, Z., Shi, H., Block, C., Bhattacharya, S., and Lu, N. (2024). Stretchable hybrid response pressure sensors. Matter *7*, 1895–1908.
5. Zhang, Y., Song, X.J., Zhang, Z.X., Fu, D.W., and Xiong, R.G. (2020). Piezoelectric Energy Harvesting Based on Multiaxial Ferroelectrics by Precise Molecular Design. Matter *2*, 697–710.
6. Li, Q., Xuan, M., Wang, A., Jia, Y., Bai, S., Yan, X., and Li, J. (2022). Biogenic sensors based on dipeptide assemblies. Matter *5*, 3643–3658.
7. Akcabay, D.T., and Young, Y.L. (2012). Hydroelastic response and energy harvesting potential of flexible piezoelectric beams in viscous flow. Phys. Fluids *24*, 054106.
8. Huang, G., Xia, Y., Dai, Y., Yang, C., and Wu, Y. (2021). Fluid–structure interaction in piezoelectric energy harvesting of a membrane wing. Phys. Fluids *33*, 063610.
9. Wang, X., Alben, S., Li, C., and Young, Y.L. (2016). Stability and scalability of piezoelectric flags. Phys. Fluids *28*, 023601.
10. Yang, W., Wen, Z., Liu, Y., Zhang, C.-a., and Stremler, M.A. (2024). Wake-induced torsional oscillation of two tethered cylinders for energy harvesting. Phys. Fluids *36*, 055129.
11. Ahmed, R.Z., Prasad, R., Kumar, M., Raj, N., Hegde, P., and Ganesh, P. (2023). Piezoelectric system on harnessing sound energy in closed environment. Phys. Fluids *35*, 117115.
12. Shen, Y., Wang, J., Wang, J., Zheng, H., Lin, K., and Xu, H. (2024). Effect of length and attack angle of the splitter plates on circular cylinder piezoelectric water energy harvester. Phys. Fluids *36*, 045131.
13. Pan, M., Yuan, C., Liang, X., Zou, J., Zhang, Y., and Bowen, C. (2020). Triboelectric and Piezoelectric Nanogenerators for Future Soft Robots and Machines. iScience *23*, 101682.
14. Machado, L.Q., Yurchenko, D., Wang, J., Clementi, G., Margueron, S., and Bartasyte, A. (2021). Multi-dimensional constrained energy optimization of a piezoelectric harvester for E-gadgets. iScience *24*, 102749.
15. Sun, Y., Yan, Y., Tian, S., Liu, G., Wu, F., Wang, P., and Gao, M. (2024). Wireless sensing in high-speed railway turnouts with battery-free materials and devices. iScience *27*, 108663.
16. Li, Y., Chen, J., Liu, S., Wang, Z., Zhang, S., Mao, C., and Wang, J. (2024). Biodegradable piezoelectric polymer for cartilage remodeling. Matter *7*, 1631–1643.
17. Tsikriteas, Z.M., Roscow, J.I., Bowen, C.R., and Khanbareh, H. (2021). Flexible ferroelectric wearable devices for medical applications. iScience *24*, 101987.
18. Mushtaq, F., Chen, X., Hoop, M., Torlakcik, H., Pellicer, E., Sort, J., Gattinoni, C., Nelson, B.J., and Pané, S. (2018). Piezoelectrically Enhanced Photocatalysis with $BiFeO_3$ Nanostructures for Efficient Water Remediation. iScience *4*, 236–246.
19. Curie, J., and Curie, P. (1880). Développement par compression de l'électricité polaire dans les cristaux hémièdres à faces inclinées. bulmi. *3*, 90–93.
20. Cady, W.G. (1947). Nature and Use of Piezoelectricity. Electr. Eng. *66*, 758–762.
21. Valasek, J. (1921). Piezo-electric and allied phenomena in Rochelle salt. Phys. Rev. *17*, 475–481.
22. Gaugain, J.M. (1859). Memoire sur l'electricite des tourmalines. Annal. Chimie Phys. *57*, 5–39.
23. Röntgen, W.C. (1883). On the thermoelectric, actinoelectric, and piezoelectric properties of quartz. London Edinburgh Philos. Mag. J. Sci. *16*, 194–197.
24. Ing, N.L., El-Naggar, M.Y., and Hochbaum, A.I. (2018). Going the distance: long-range conductivity in protein and peptide bioelectronic materials. J. Phys. Chem. B *122*, 10403–10423.
25. Bayley, S.T. (1951). The dielectric properties of various solid crystalline proteins, amino acids and peptides. Trans. Faraday Soc. *47*, 509–517.
26. Gent, W.L.G. (1954). Dielectric properties of aqueous solutions of amino acids, polypeptides and proteins. Part 1.—Behaviour of glycine solutions at 300 Mc/s. Trans. Faraday Soc. *50*, 1229–1235.
27. Rosenberg, B. (1962). Electrical conductivity of proteins. Nature *193*, 364–365.
28. Guerin, S., Tofail, S.A.M., and Thompson, D. (2018). Longitudinal Piezoelectricity in Orthorhombic Amino Acid Crystal Films. Cryst. Growth Des. *18*, 4844–4848.
29. Kim, D., Han, S.A., Kim, J.H., Lee, J.H., Kim, S.W., and Lee, S.W. (2020). Biomolecular Piezoelectric Materials: From Amino Acids to Living Tissues. Adv. Mater. *32*, 1906989.
30. Vasilescu, D., Cornillon, R., and Mallet, G. (1970). Piezoelectric Resonances in Amino-acids. Nature *225*, 635.
31. Chorsi, M.T., Le, T.T., Lin, F., Vinikoor, T., Das, R., Stevens, J.F., Mundrane, C., Park, J., Tran, K.T.M., Liu, Y., et al. (2023). Highly piezoelectric, biodegradable, and flexible amino acid nanofibers for medical applications. Sci. Adv. *9*, eadg6075.
32. Guerin, S., Stapleton, A., Chovan, D., Mouras, R., Gleeson, M., McKeown, C., Noor, M.R., Silien, C., Rhen, F.M.F., Kholkin, A.L., et al. (2018). Control of piezoelectricity in amino acids by supramolecular packing. Nat. Mater. *17*, 180–186.
33. Jeon, B., Han, D., and Yoon, G. (2023). Piezoelectric characteristics of PVA/DL-alanine polycrystals in d33 mode. iScience *26*, 105768.
34. Zhang, W., Chen, X., Wang, Y., Wu, L., and Hu, Y. (2020). Experimental and Modeling of Conductivity for Electrolyte Solution Systems. ACS Omega *5*, 22465–22474.
35. Saha, S., Ray, T., Basak, S., and Roy, M.N. (2016). NMR, surface tension and conductivity studies to determine the inclusion mechanism: thermodynamics of host–guest inclusion complexes of natural amino acids in aqueous cyclodextrins. New J. Chem. *40*, 651–661.
36. Zhuo, K., Chen, Y., Kang, L., Xu, S., and Wang, J. (2009). Dielectric constants for binary amino acid– water solutions from (278.15 to 313.15). J. Chem. Eng. Data *54*, 137–141.
37. Krishnamurti, K., and Kate, S.R. (1951). Changes in Electrical Conductivity during Bacterial Growth. Nature *168*, 170.
38. Cardew, M.H., and Eley, D.D. (1959). The semiconductivity of organic substances. Part 3.—Haemoglobin and some amino acids. Tras. Faraday Soc. *27*, 115–128.
39. Amit, M., Appel, S., Cohen, R., Cheng, G., Hamley, I.W., and Ashkenasy, N. (2014). Hybrid proton and electron transport in peptide fibrils. Adv. Funct. Mater. *24*, 5873–5880.
40. Piperno, S., Mirzadeh, E., Mishuk, E., Ehre, D., Cohen, S., Eisenstein, M., Lahav, M., and Lubomirsky, I. (2013). Water-induced pyroelectricity from nonpolar crystals of amino acids. Angew. Chem. Int. Ed *52*, 6513–6516.

41. Agam, Y., Nandi, R., Bulava, T., and Amdursky, N. (2021). The role of the protein–water interface in dictating proton conduction across protein-based biopolymers. Mater. Adv. *2*, 1739–1746.
42. Sterpone, F., Stirnemann, G., Hynes, J.T., and Laage, D. (2010). Water Hydrogen-Bond Dynamics around Amino Acids: The Key Role of Hydrophilic Hydrogen-Bond Acceptor Groups. J. Phys. Chem. B *114*, 2083–2089.
43. Sebben, D., and Pendleton, P. (2014). Infrared spectrum analysis of the dissociated states of simple amino acids. Spectrochim. Acta *132*, 706–712.
44. Schwaminger, S.P., García, P.F., Merck, G.K., Bodensteiner, F.A., Heissler, S., Günther, S., and Berensmeier, S. (2015). Nature of interactions of amino acids with bare magnetite nanoparticles. J. Phys. Chem. C *119*, 23032–23041.
45. Adhikari, S., and Kar, T. (2012). Bulk single crystal growth and characterization of l-leucine–A nonlinear optical material. Mater. Chem. Phys. *133*, 1055–1059.
46. Prabhu, M.D., Tonannavar, J., and Tonannavar, J. (2021). Multiple-H-bonded-zwitterionic tetramer structure for L-(+)-2-chlorophenylglycine, as investigated by UV, IR and Raman spectroscopy and electronic structure calculations. J. Mol. Struct. *1246*, 131218.
47. Yi, B., Yu, L., Tang, H., Wang, W., Liu, W., and Zhang, Y. (2021). Lysine-doped polydopamine coating enhances antithrombogenicity and endothelialization of an electrospun aligned fibrous vascular graft. Appl. Mater. Today *25*, 101198.
48. Mahadevan, M., Magesh, M., Ramachandran, K., Anandan, P., Arivanandhan, M., and Hayakawa, Y. (2014). Synthesis, growth, crystal structure and characterization of a new organic NLO crystal: l-Lysine 4-nitrophenolate monohydrate (LLPNP). Spectrochim. Acta *130*, 416–422.
49. Rao, C.N.R., Rao, K.G., Goel, A., and Balasubramanian, D. (1971). Configuration of secondary amides and thioamides: spectroscopic and theoretical studies. J. Chem. Soc. A. *A*, 3077–3083.
50. Boukaoud, A., Chiba, Y., and Sebbar, D. (2021). A periodic DFT study of IR spectra of amino acids: An approach toward a better understanding of the NH and OH stretching regions. Vib. Spectrosc. *116*, 103280.
51. Chowdhry, B.Z., Dines, T.J., Jabeen, S., and Withnall, R. (2008). Vibrational spectra of α-amino acids in the zwitterionic state in aqueous solution and the solid state: DFT calculations and the influence of hydrogen bonding. J. Phys. Chem. A *112*, 10333–10347.
52. Gómez-Zavaglia, A., and Fausto, R. (2003). Low-temperature solid-state FTIR study of glycine, sarcosine and N, N-dimethylglycine: observation of neutral forms of simple α-amino acids in the solid state. Phys. Chem. Chem. Phys. *5*, 3154–3161.
53. Williams, P.A., Hughes, C.E., and Harris, K.D.M. (2015). L-Lysine: Exploiting Powder X-ray Diffraction to Complete the Set of Crystal Structures of the 20 Directly Encoded Proteinogenic Amino Acids. Angew. Chem. Int. Ed. *54*, 3973–3977.
54. Huo, Q., Dziri, L., Desbat, B., Russell, K.C., and Leblanc, R.M. (1999). Polarization-modulated infrared reflection absorption spectroscopic studies of a hydrogen-bonding network at the air– water interface. J. Phys. Chem. B *103*, 2929–2934.
55. Bouchet, A., Schütz, M., Chiavarino, B., Crestoni, M.E., Fornarini, S., and Dopfer, O. (2015). IR spectrum of the protonated neurotransmitter 2-phenylethylamine: dispersion and anharmonicity of the NH 3+–π interaction. Phys. Chem. Chem. Phys. *17*, 25742–25754.
56. Chen, C., Huang, C., Waluyo, I., Nordlund, D., Weng, T.C., Sokaras, D., Weiss, T., Bergmann, U., Pettersson, L.G.M., and Nilsson, A. (2013). Solvation structures of protons and hydroxide ions in water. J. Chem. Phys. *138*, 154506.
57. Śmiechowski, M., and Stangret, J. (2007). Hydroxide Ion Hydration in Aqueous Solutions. J. Phys. Chem. A *11*, 2889–2897.
58. Shi, L., Gruenbaum, S.M., and Skinner, J.L. (2012). Interpretation of IR and Raman Line Shapes for H2O and D2O Ice Ih. J. Phys. Chem. B *116*, 13821–13830.
59. Henao, A., Ruiz, G.N., Steinke, N., Cerveny, S., Macovez, R., Guàrdia, E., Busch, S., McLain, S.E., Lorenz, C.D., and Pardo, L.C. (2020). On the microscopic origin of the cryoprotective effect in lysine solutions. Phys. Chem. Chem. Phys. *22*, 6919–6927.
60. Soper, A.K., and Benmore, C.J. (2008). Quantum Differences between Heavy and Light Water. Phys. Rev. Lett. *101*, 065502.
61. De Marco, L., Carpenter, W., Liu, H., Biswas, R., Bowman, J.M., and Tokmakoff, A. (2016). Differences in the Vibrational Dynamics of H_2O and D_2O: Observation of Symmetric and Antisymmetric Stretching Vibrations in Heavy Water. J. Phys. Chem. Lett. *7*, 1769–1774.
62. Génin, F., Quilès, F., and Burneau, A. (2001). Infrared and Raman spectroscopic study of carboxylic acids in heavy water. Phys. Chem. Chem. Phys. *3*, 932–942.
63. Adhikari, U., and Scheiner, S. (2013). Magnitude and mechanism of charge enhancement of CH·· O hydrogen bonds. J. Phys. Chem. A *117*, 10551–10562.
64. Scheiner, S., Kar, T., and Gu, Y. (2001). Strength of the CαH·· O hydrogen bond of amino acid residues. J. Biol. Chem. *276*, 9832–9837.
65. Madejová, J., Sekeráková, Ľ., Bizovská, V., Slaný, M., and Jankovič, Ľ. (2016). Near-infrared spectroscopy as an effective tool for monitoring the conformation of alkylammonium surfactants in montmorillonite interlayers. Vib. Spectrosc. *84*, 44–52.
66. Filopoulou, A., Vlachou, S., and Boyatzis, S.C. (2021). Fatty Acids and Their Metal Salts: A Review of Their Infrared Spectra in Light of Their Presence in Cultural Heritage. Molecules *26*, 6005.
67. Elbagerma, M.A., Edwards, H.G.M., Munshi, T., Hargreaves, M.D., Matousek, P., and Scowen, I.J. (2010). Characterization of new cocrystals by Raman spectroscopy, powder X-ray diffraction, differential scanning calorimetry, and transmission Raman spectroscopy. Cryst. Growth Des. *10*, 2360–2371.
68. Carrier, D., and Pézolet, M. (1984). Raman spectroscopic study of the interaction of poly-l-lysine with dipalmitoylphosphatidylglycerol bilayers. Biophys. J. *46*, 497–506.
69. Soman, J., Suresh, C.G., and Vijayan, M. (1988). X-ray studies on crystalline complexes involving amino acids and peptides. Int. J. Pept. Protein Res. *32*, 352–360.
70. Hyde, S.T. (2001). Identification of lyotropic liquid crystalline mesophases. In Handbook of applied surface and colloid chemistry, K. Holmberg, ed. (Wiley), pp. 299–332.
71. Newman, B.A., Yoon, C.H., Pae, K.D., and Scheinbeim, J.I. (1979). Piezoelectric activity and field-induced crystal structure transitions in poled poly (vinylidene fluoride) films. J. Appl. Phys. *50*, 6095–6100.
72. Wang, W., Fan, H., and Ye, Y. (2010). Effect of electric field on the structure and piezoelectric properties of poly (vinylidene fluoride) studied by density functional theory. Polymer *51*, 3575–3581.
73. Kisi, E.H., Piltz, R.O., Forrester, J.S., and Howard, C.J. (2003). The giant piezoelectric effect: electric field induced monoclinic phase or piezoelectric distortion of the rhombohedral parent? J. Phys. Condens. Matter *15*, 3631–3640.
74. Park, S.-E., and Shrout, T.R. (1997). Ultrahigh strain and piezoelectric behavior in relaxor based ferroelectric single crystals. J. Appl. Phys. *82*, 1804–1811.
75. Li, G., Liu, Y., Xu, W., Song, A., and Hao, J. (2014). Transition of Phase Structures in Mixtures of Lysine and Fatty Acids. J. Phys. Chem. B *118*, 14843–14851.
76. Tushar, C., Ralish, R., Rajesh, M., Manikandan, M., Rajapandi, R., Kar, V.R., and Jayakrishna, K. (2019). Maintenance and monitoring of composites. In Structural Health Monitoring of Biocomposites, Fibre-Reinforced Composites and Hybrid Composites (Woodhead Publishing).
77. Pye, C.C., Ziegler, T., van Lenthe, E., and Louwen, J.N. (2009). An implementation of the conductor-like screening model of solvation within the Amsterdam density functional package. Part II. COSMO for real solvents. Can. J. Chem. *87*, 790–797.
78. Demsar, J., Curk, T., Erjavec, A., Gorup, C., Hocevar, T., Milutinovic, M., Mozina, M., Polajnar, M., Toplak, M., Staric, A., et al. (2013). Orange: Data Mining Toolbox in Python. J. Mach. Learn. Res. *14*, 2349–2353.
79. Toplak, M., Read, S.T., Sandt, C., and Borondics, F. (2021). Quasar: easy machine learning for biospectroscopy. Cells *10*, 2300.
80. Von Dreele, R.B. (2014). Small-angle scattering data analysis in GSAS-II. J. Appl. Crystallogr. *47*, 1784–1789.
81. Toby, B.H., and Von Dreele, R.B. (2013). GSAS-II: the genesis of a modern open-source all purpose crystallography software package. J. Appl. Crystallogr. *46*, 544–549.
82. Leontowich, A.F.G., Gomez, A., Diaz Moreno, B., Muir, D., Spasyuk, D., King, G., Reid, J.W., Kim, C.Y., and Kycia, S. (2021). The lower energy diffraction and scattering side-bounce beamline for materials science at the Canadian Light Source. J. Synchr. Rad. *28*, 961–969.
83. Levenberg, K. (1944). A Method for the Solution of Certain Non-Linear Problems in Least Squares. Q. Appl. Math. *2*, 164–168.
84. Marquardt, D.W. (1963). An Algorithm for Least-Squares Estimation of Nonlinear Parameters. J. Soc. Ind. Appl. Math. *11*, 431–441.

STAR★METHODS

KEY RESOURCES TABLE

REAGENT or RESOURCE	SOURCE	IDENTIFIER
Chemicals, peptides, and recombinant proteins		
L-lysine	Sigma Aldrich Canada	Cat# L5501
L-arginine	Sigma Aldrich Canada	Cat# A5006
L-serine	Fisher Scientific Canada	Cat# S003525G
L-threonine	Fisher Scientific Canada	Cat# AAA1685114
L-histidine	Fisher Scientific Canada	Cat# AC166150250
D-alanine	Fisher Scientific Canada	Cat# A017725G
Oleic acid	Sigma Aldrich Canada	Cat# 364525
Software and algorithms		
COSMO-RS	SCM	http://www.scm.com
ImageJ	https://imagej.net/ij/	https://doi.org/10.1038/nmeth.2089
Quasar Orange	Orange	https://quasar.codes/
Prism 10.1	GraphPad Software, San Diego, CA	https://www.graphpad.com/
Microsoft Excel 2016	Microsoft	Version 2405

RESOURCE AVAILABILITY

Lead contact

Further information and requests for resources and reagents should be directed to and will be fulfilled by the lead contact, Erica Pensini (epensini@uoguelph.ca).

Materials availability

This study did not generate new unique reagents. L-lysine (purity ≥98%) and L-arginine (purity ≥98%), as well as oleic acid (90% purity) were purchased from Sigma Aldrich (Canada). Other amino acids tested include L-serine (99% pure, Thermo), L-threonine and L-histidine (both 98% pure, Thermo), D-alanine (>98% pure, TCI America), all purchased from Fisher Scientific. Milli-Q was used in all experiments conducted. Milli-Q water was obtained using Milli-Q Equation 7000 Ultrapure Water Purification System (Sigma Aldrich, Canada).

Data and code availability

- All data can be obtained from the lead contact, provided the request is reasonable.
- This paper does not report original code.
- Activity coefficients of amino acids and water in binary mixtures were estimated using COSMO-RS, version 2023.1 (http://www.scm.com) was developed by Vrije Universiteit, Amsterdam.[77] ImageJ (https://doi.org/10.1038/nmeth.2089) is a free software developed by the National Institutes of Health and the Laboratory for Optical and Computational Instrumentation, LOCI (University of Wisconsin). ATR-FTIR spectra were processed using Quasar Orange, which is a freely available software.[78,79] SAXS patterns were processed with GSASII (Argonne National Laboratory (C), 2010).[80,81] Excel (Microsoft corporation) was used to process cyclic voltammetry data and shear rheology data, to obtain averages and standard deviations based on at least two replicates.
- Any additional information required to reanalyze the data reported in this paper is available from the lead contact upon request.

EXPERIMENTAL MODEL AND STUDY PARTICIPANT DETAILS

The experimental model details are fully described in the main text (See section "results"). We did not use humans or animals in the study (there are no participants).

METHOD DETAILS

Attenuated total reflectance- Fourier transform infrared spectroscopy (ATR-FTIR)

ATR-FTIR measurements were conducted to analyze mixtures containing L-lysine and oleic acid, L-lysine and water, as well as ternary mixtures containing L-lysine, oleic acid and water. Absorbance spectra were collected using an ATR-FTIR spectrometer (Thermoscientific Nicolet

Summit FTIR spectrometer with an Everest ATR), with an accompanying IR solution software. Each spectrum is the average of 20 scans, with a resolution of 2 cm^{-1}, in the wavenumber range of 400 cm^{-1} to 4000 cm^{-1}.

Conductivity measurements of mixtures of amino acids in water

Conductivity measurements of mixtures containing varying concentrations of L-lysine and L-arginine in water were conducted using a Thermo Scientific Orion Star A212 Conductivity Benchtop Meter. Each measurement was conducted three or more times at 20°C.

Cyclic voltammetry experiments

Cyclic voltammetry experiments were conducted using piezoelectric materials prepared with equimolar ratios of lysine or arginine, oleic acid, and varying water percentages, in a three-electrode cell using a 1.2 cm^2 graphite rod as a working electrode, Pt counter electrode, and a Ag/AgCl reference electrode. The voltage range was from −0.3 V to 0.5 V, with scan rates varied from 10, 20, 50 and 100 mV/s. The sampling interval was 0.001 V, with a pause of 2 s between steps. Measurements were conducted using a CHI660E workstation (CH instruments).

Shear rheology and viscosity measurements

Shear rheology experiments were conducted at 23°C using a rotational torque-controlled (i.e., combined-motor-transducer type) rheometer (MCR302 Anton Paar, Graz, Austria). Experiments were conducted with a parallel plate geometry (diameter = 50 mm), using samples containing equimolar amounts of either L-lysine or L-arginine and oleic acid, and varying amounts of water (up to 89 wt %). Two sets of rheology measurements were conducted: strain amplitude sweeps and frequency sweeps. Strain amplitude sweeps were conducted at a frequency of 6 rad/s, and a strain ranging from 1%–1000%. Frequency sweeps were conducted at a frequency ranging from 1 to 100 rad/s, at a strain at which G′ and G″ are independent of it. This strain was identified in strain sweeps, and depended on the gel analyzed.

Powder X-ray diffraction

Powder XRD measurements were conducted on samples prepared with equimolar amounts of oleic acid and L-lysine, without water and with 90 wt % water. Measurements were also conducted using equimolar ratios of L-arginine and oleic acid, and varying water percentages. Measurements were conducted using a Rigaku MiniFlex 300/600 equipped with a BTS 150 chamber and a D/teX Ultra2 detector. The X-ray generator operated at 40 kV and 15 mA. The step width was 0.01° and the scan speed was 3.00°/min. The scan range was 2θ = 2–35°.

Polarized light microscopy

Samples were imaged by polarized light microscopy on an OMAX optical microscope model M838PL (OMAX Microscope, USA) using a 10X, 20X, 40X, and 100× objective lens. Images were captured using a model A35180U3 digital camera (OMAX Microscope, USA) using Toupview software (ToupTek Photonics, Zhejiang, China).

Synchrotron based small angle X-Ray scattering

We used SAXS to analyze samples containing equimolar ratios of L-lysine and oleic acid, either without water or with varying water percentages. Samples were analyzed either with no electric fields applied, or by applying electric fields of varying intensity. SAXS experiments were carried out at the Canadian Light Source Synchrotron (CLS) on the Brockhouse Diffraction Sector Wiggler Low Energy Beamline (BXDS-WLE).[82] Samples were sandwiched between tape (e.g., Scotch tape). Tape does not contribute any peaks in the region analyzed (cf. Figure S1, supplemental information file), and is thus a suitable material. SAXS data were collected with a Rayonix MX300 detector, which consists of a 4 x 4 fused array of fiber-optic tapers bonded to CCDs, with 300 x 300 mm^2 square active area, without gaps in the imaging area. Full resolution is 8192 x 8192 pixels. SAXS patterns were collected with a photon energy of 18.8 keV (λ = 0.6595 Å), and sample-to-detector distance of 233 cm. SAXS patterns were collected in transmission geometry with a 120 s dwell time. Patterns were processed with GSASII (Argonne National Laboratory (C), 2010). This product includes software developed by the UChicago Argonne, LLC).[80,81] SAXS data were calibrated with silver behenate (AgBeh) and instrument parameters such as sample-to-detector distances, detector tilt, beam center, were refined as described elsewhere.[80] Briefly, these were optimized to enable analysis over the desired q range, thereby enabling observation of samples at small angles. SAXS patterns were integrated from q = 0.015 to q = 0.929 $Å^{-1}$, where q is the magnitude of the scattering vector: $q=(4\pi/\lambda)\sin(\theta/2)$, where λ is the wavelength of the X-rays and θ the scattering angle. Measurements were done at least in duplicate for each sample. Moreover, SAXS images were processed using ImageJ (https://doi.org/10.1038/nmeth.2089), which was developed by the National Institutes of Health and the Laboratory for Optical and Computational Instrumentation, LOCI (University of Wisconsin) and the Radial_Profile_Angle Plugin, originally developed by Paul Baggethun and extended by Phillippe Carl (http://questpharma.u-strasbg.fr/html/radial-profile-ext.html). This plugin produces a profile plot of normalized integrated intensities around concentric circles as a function of the azimuthal angle. The data obtained using ImageJ and this plugin were fitted to two Gaussian curves by nonlinear regression using Prism 10.1 (GraphPad Software, San Diego, CA). We used a standard nonlinear regression routine.[83,84]

Modeling of conductivity data

Conductivity data were described using the model (1) developed by Zhang et al.[34]:

$$k = (P_1 T + P_2) m^n \exp\left(-\frac{P_3 m}{T - P_4}\right) \quad \text{(Equation 1)}$$

where m is the molar concentration of the electrolyte, and P_1, P_2, P_3, P_4, and n are constants. These constants are independent of electrolyte concentration and temperature, but dependent on the solvent composition.

Specifically, the value of n describes the nonlinear relationship between the concentration of free ions and the concentration of the electrolyte in the solution caused by ionic association at medium or high concentrations. When $n = 1$, the relationship between the concentration of free ions and the concentration of the electrolyte is linear. When n differs from 1, their relationship is not linear. The value of n is related to the dielectric constant on the medium. In particular, n is larger in solvents with a low dielectric constant, while n is typically between 0.5 and 1.2 in solvents with a high the dielectric constant. The rationale for this is that solvents with low dielectric constants are more likely to form nonconductive ion pairs, thereby decreasing the number of free ions which partake in conduction in the solution. When the solvent has a high dielectric constant, the electrolyte is completely or almost completely dissociated, and n is close to 1.

Estimate of piezoelectric coefficients

The piezoelectric coefficient measures the volume change occurring when a piezoelectric material is subjected to an electric field.[76] We estimated the piezoelectric coefficient of a material containing equimolar ratios of lysine and oleic acid, and 91 wt % water. Materials were exposed to 5 V and 10 V, using a Gw Instek GPS-3030DD DC power supply, and steel electrodes having a 1 mm diameter. Materials were confined in glass cells having a 1 mm thickness, and they were either also confined laterally or allowed to deform along the xy plane. The materials were imaged under an VHX digital microscope (Keyence, Canada), to monitor volume changes in real time while subjecting the materials to an electric field. Knowing that samples were confined along the z axis (to 1 mm thickness), volumes were estimated based on the area seen in the xy plane by processing microscopy images with ImageJ (https://doi.org/10.1038/nmeth.2089). ImageJ was developed by the National Institutes of Health and the Laboratory for Optical and Computational Instrumentation, LOCI (University of Wisconsin). ImageJ was also used to determine the electrode distance, to estimate the electric field based on the applied voltage.

QUANTIFICATION AND STATISTICAL ANALYSIS

To determine the azimuthal angle, the data obtained using ImageJ and this plugin were fitted to two Gaussian curves by nonlinear regression using Prism 10.1 (GraphPad Software, San Diego, CA). We used a standard nonlinear regression routine.[83,84] All statistical parameters are provided in the supplemental information file (Tables S2–S5, supplemental information file). SAXS experiments were conducted in duplicate.

To fit conductivity data to the model developed by Zhang et al., we also used Prism 10.1 (GraphPad Software, San Diego, CA) and a standard nonlinear regression routine.[83,84] Each data point was the average of at least three independent measurements. We provide the average and standard deviation in Figure 1.

All ATR-FTIR experiments were conducted in duplicate at least, to obtain the averages and standard deviations shown in Figure 3 are reported in Table S1 (supplemental information file). ATR-FTIR data were processed using Orange Quasar (see key resources table).

To determine piezoelectric coefficients, we conducted three independent experiments. In each case, the deformation differed, depending on the time for which an electric field was applied, as seen in Figure 12 and 13 shown in the paper. The different results obtained are presented. Additional experiments (two independent tests) gave similar results, but are not shown for brevity.

Shear rheology and cyclic voltammetry measurements were conducted in duplicate at least, and sample representative strain and frequency sweeps are shown in the paper. Averages and standard deviations were obtained using Excel.

Polarized light microscopy samples were prepared in duplicate, and observed in different regions. Representative images are shown in the paper. We do not report averages and standard deviations from these measurements.